University of Alberta

CONSERVATIVE FORMULATION FOR HYDRAULIC MODELLING IN NATURAL OPEN CHANNELS

by

JIE CHEN 

A thesis submitted to the Faculty of Graduate Studies and Research in partial fulfillment of the requirements for the degree of **Master of Science**

in
Water Resources Engineering
Department of Civil and Environmental Engineering

Edmonton, Alberta
Spring, 2006

Your file Votre référence
ISBN: 0-494-13802-5
Our file Notre référence
ISBN: 0-494-13802-5

ABSTRACT

This investigation considers a modified formulation of the St. Venant equations for natural channels, which has been manipulated into a fully conservative form by revising the momentum flux term accounting for the topographic variation in the momentum equation. The accuracy implications for this approximate formulation are examined using an error analysis. Furthermore, an energy loss analysis is performed to illustrate the validation of the approximate formulation. Instead of using the average water surface elevation, a general formula is proposed to calculate the constant water surface elevation when evaluating the pressure acting on the wetted boundary surface. Using the Characteristic-Dissipative-Galerkin finite element scheme, accurate results are obtained for hydraulic jumps and steep surge wave propagation. Application of the model is illustrated for flood routing of the 1995 event on the Oldman River in southern Alberta. The computational results are in good agreement with the observed data.

ACKNOWLEDGEMENTS

This research was supported through funding from the Natural Sciences and Engineering Research Council of Canada, Alberta Environment (Water Research Users Group) and the University of Alberta. (FS Chia scholarship). This support is most gratefully acknowledged. Thanks are also extended to Chandra Mahabir and Jim Choles of the River Engineering group at Alberta Environment for their support, assistance and advice on the Oldman River modelling component.

The author would like to express special thanks to his supervisors Dr.Faye E.Hicks and Dr. Peter Steffler, who supervised the research and provided much valuable advice. Their keen interest and understanding of topic led to the success and accomplishment of the study. Their guidance and encouragement are greatly appreciated. Dr. G. Reuter is specially thanked for his contributions in reviewing this thesis. Also, Nedal Barbar for his help with the Oldman river database as well as Perry Fedun for assistance by providing computer support are gratefully acknowledged.

The author would like to express warm thanks to his family. Their unselfish support and encouragement is gratefully acknowledged.

TABLE OF CONTENTS

LIST OF TABLES

LIST OF FIGURES

NOTATION

A wetted cross-sectional area;

$\mathbf{A}$ convection matrix;

ΔA difference of wetted area;

b channel width at elevation z ;

B bottom width of channel;

B_1, B_2 bottom width at section 1 and 2, respectively;

C_* non- dimensional Chezy coefficient;

$\mathbf{F}$ flux vector;

F_1 Froude number at section 1;

$\mathbf{G}_c$ source term of conservative forms;

$\mathbf{G}_n$ source term of non-conservative forms;

$\mathbf{f}$ source vector;

f_i basis function;

g gravitational acceleration;

g_i upwinding function;

h water depth;

$\overline{h}$ constant water depth over control volume;

$\overline{h}_c$ depth from the free surface to the centroid of difference of area;

h_d downstream water depth;

h_f local head loss;

h_u upstream water depth;

H elevation of water surface (stage);

H_1, H_2 water surface elevation (stage) at location x_1 and x_2, respectively;

$\bar{H}$ average stage within control volume;

I_1 first moment of the wetted cross section with respect to the free surface;

I_2 spatial variation of first moment;

$I_{1\bar{H}}$ first moment of the wetted cross section with respect to the average free surface $\bar{H}$;

$\mathbf{K}$ stiffness matrix;

K local loss coefficient;

L boundary of domain;

l_e left boundary location of element;

m side slope of the trapezoidal channel;

N_e number of elements;

$\mathbf{N}_i$ basis function matrix;

n_x x component of unit vector outward normal to Γ_0;

p pressure acting on bottom boundaries;

$p_{\bar{H}}$ pressure acting on bottom boundaries with average constant free surface $\bar{H}$;

$P_{\max}$ maximum end pressure force;

P_1, P_2 pressure force at section 1 and 2, respectively;

P' pressure force at side wall;

Q discharge;

r_e right boundary location of element;

R hydraulic radius;

$\mathbf{S}$ mass matrix;

S_B divergent slope of side wall;

S_f friction slope;

S_o bed slope;

S_W slope of water surface;

t temporal coordinate;

U average cross-sectional velocity;

V_1, V_2 velocity at section 1 and 2, respectively;

v_i test function;

$\mathbf{W}$ upwind matrix;

x space coordinate;

x_1, x_2 left and right boundary of the control volume;

z depth integration variable;

z_o lowest elevation of the cross section;

z_1 Bed elevation at cross section x_1;

Γ_S side wall boundary;

Γ_B bed boundary;

Γ_o wetted boundary surface;

$\mathbf{\Phi}$ solution vector;

α weighting coefficient;

ε absolute error;

ε_p relative error;

ε_S error in pressure force of side wall owing to width variation;

φ the angle the bed makes with the horizontal;

θ implicitness;

ρ density of water;

τ x component of the boundary shear stress;

ω upwinding coefficient;

Δx space step;

Δt time step.

CHAPTER 1

INTRODUCTION

Over the past few decades, considerable attention has be addressed to the development of stable, accurate shock capturing schemes for the numerical solution of the Saint Venant equations for one-dimensional dynamic open channel flows (Liggett and Cunge 1975; Katopodes 1984; Fennema and Chaudhry 1987; Hicks and Steffler 1994; Tseng *et al.* 2001). However, the primary effort has focused on simple channel geometries, most typically rectangular cross sections, whereas natural channel geometries present the more common scenario in practical applications.

The main issue in extending the previous work to natural channel application is in terms of momentum conservation. For the rectangular channel case, investigators have found that conservative formulations generally provide more stable and accurate solutions than non-conservative formulations, due to better conservation accuracy (Hicks and Steffler 1994). This is particularly important when modeling highly dynamic events, such as dam break floods or ice jam release surge propagation. Therefore, it is desirable to discretize a conservative formulation of St.Venant equations for propagating shocks. Although a number of conservative formulations of the St. Venant equations can be derived for the simple rectangular channel case, a fully conservative formulation for natural channel geometries does not exist due to its irregular topography (Blackburn 2000). Consequently, much of the numerical research has focused on developing numerically robust solution schemes which display stable and accurate solutions for the conventional

natural channel formulations (Garcia-Navarro and Vazquez-Cendon 2000; Sanders 2001; Tseng *et al.* 2001; Sanders *et al.* 2003; Ying *et al.* 2004) To implement a conservative formulation in natural channel, a key problem is the treatment of irregular bathymetry, namely the treatment of the source terms accounting for the hydrostatic pressure force caused by the longitudinal width variation and bed slope.

Sanders (2001) introduced a scheme to solve the St. Venant equations using a Godunov-type finite volume, in which bed slope and variable channel width effects are treated as source, rather than flux, terms. The source term accounting for varying channel width is quantifies the hydrostatic pressure exerted by the sidewalls by assuming a constant depth within the control volume. The constant depth used in this calculation is the depth at the centre of the control volume (as shown in Figure 1.1). Sanders did not assume this constant depth in treating the source term associated with the bed slope.

Capart *et al.* (2003) undertook a different approach, proposing a fully conservative approximation to the natural channel equations, and solving it with a finite volume method. Unlike Sanders (2001) treatment, in which a constant water depth is assumed in the control volume, in the Capart *et al.* (2003) approximation, a constant water surface elevation is assumed throughout the control volume (shown in Figure 1.2). Rather than treating the irregular geometry effects as source terms, they modified the momentum flux term to account for channel slope and variation of sidewall. (Capart *et al.* 2003). This approach leads to a formulation which defaults to a fully conservative form for the simple case of rectangular channels of constant width, and in the case of a horizontal water

surface (for any geometry). For the natural channel case with non-horizontal water surface slope, the error is negligible for mild channel slopes and small sidewall inclination (Capart *et al.* 2003). They validated their model for the steady flow case of a hydraulic jump in an expanding channel and the unsteady flow case of a dam break wave propagating over a dry bed. As Capart *et al.*'s (2003) approximate formulation is a fully conservative formulation; it may have some numerical advantages.

In this investigation, the validity of Capart *et al.*'s (2003) approximate formulation is further investigated by quantifying the limits of applicability for practical situations. The formulation proposed by Capart *et al.* (2003) adapts ideally to solution by the finite element method, and this is illustrated by solving the equations using the Characteristic-Dissipative-Galerkin (CDG) finite element scheme (Hicks and Steffler 1992). Model simulations are used together with the error relationship, to quantify the error associated with cases of extreme water surface slope and sidewall inclination.

Chapter 2 presents detailed development of the numerical model, which is called RIVER1D. Firstly, the derivation of the approximate momentum equation used in RIVER1D is illustrated. An error analysis is then conducted for the case of a rectangular channel of variable width, and an approach for arbitrary channel geometries is suggested. Also, an energy loss analysis for the approximate formulation is performed for sudden expansions and contractions in rectangular channels. The detailed CDG finite element implementation is also presented.

Chapter 3 deals with the validation of the proposed model for both steady flow and unsteady flow. In the steady flow case, transition from a mild to a steep slope is modeled to demonstrate the robust handling of transcritical flows. Then, a hydraulic jump in an expanding channel is simulated, and compared to Capart *et al.*'s (2003) solution of the same problem. For the unsteady flow case, a classical dam break situation is simulated to demonstrate the shock capturing ability of the proposed model. Further, the unsteady flow simulation is extended to model a dam break in a converging and diverging channel, comparing to the experimental results of Bellos *et al.* (1992).

In chapter 4, the application of the RIVER1D model to an actual natural river is demonstrated, performing a flood routing simulation in Oldman River in southern Alberta for the 1995 (1:100) flood event. A sensitivity analysis is conducted as well. The results are compared to Water Survey of Canada (WSC) gauging records and field survey data obtained from Alberta Environment. Chapter 5 summarizes the conclusions of this study, and provides recommendations for further research.

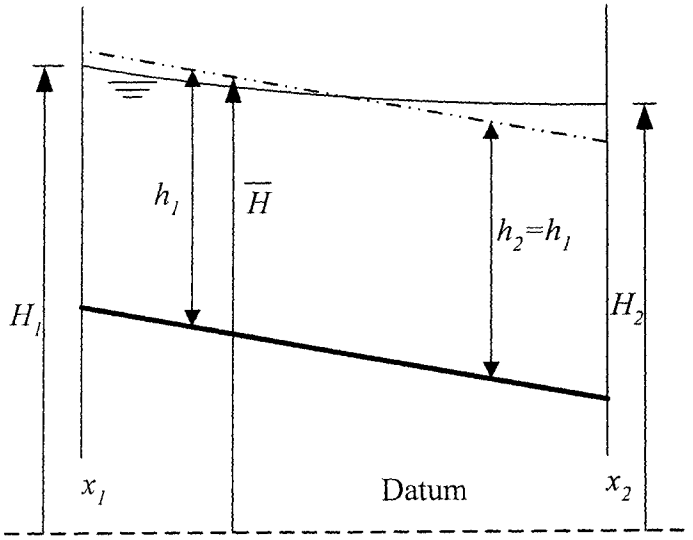

Figure 1.1 Approximate water surface profile used by Sander (2001).

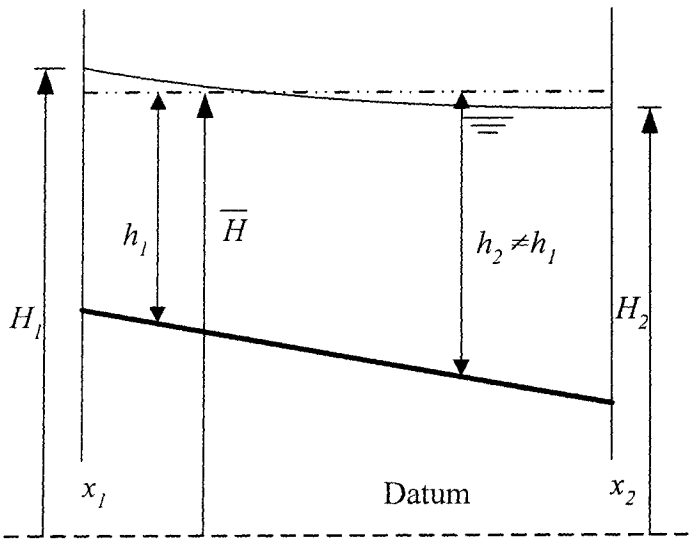

Figure 1.2 Approximate water surface profile used by Capart *et al.* (2003).

CHAPTER 2

NUMERICAL MODEL DEVELOPMENT

2.1 Equation Formulation

Based on conservation of mass and longitudinal momentum principles (control volume as shown in Figure 2.1), the St.Venant equations describing one-dimension unsteady flow in an open channel are written as (Cunge *et al.* 1980):

$$\frac{\partial A}{\partial t}+\frac{\partial Q}{\partial x}=0 \tag{2.1}$$

$$\frac{\partial Q}{\partial t}+\frac{\partial}{\partial x}\left(\frac{Q^2}{A}+gI_1\right)=gA\left(S_o-S_f\right)+gI_2 \tag{2.2}$$

in which, I_1 is the first moment of the wetted cross section with respect to the free surface

$$I_1=\int_{z_o}^{H}(H-z)b(x,z)\,dz \tag{2.3}$$

and I_2 is the spatial variation of the first moment:

$$I_2=\int_{z_o}^{H}(H-z)\frac{\partial b(x,z)}{\partial x}dz \tag{2.4}$$

Here, A= cross-sectional area perpendicular to the flow, Q= discharge, H = elevation of the water surface, h= water depth, S_o= bed slope, S_f= friction slope, g=gravitational acceleration, z_o= lowest elevation of the cross section and $b(x,z)$=channel width at elevation z.

These equations were derived based on the following assumptions:

(1) The flow is one dimensional and the water level across the section is horizontal.

(2) The pressure distribution is hydrostatic.

(3) The velocity distribution is uniform over the cross section.

(4) The effect of boundary friction in unsteady flow can be accounted for through resistance laws applicable for steady flow.

(5) The variables Q and A are continuous differentiable functions.

(6) The bed slope is small so that sin φ =tan φ, where φ is the angle the bed makes with the horizontal.

For a trapezoidal channel

$$I_1 = h^2\left(\frac{B}{2}+\frac{hm}{3}\right) \tag{2.5}$$

$$I_2 = h^2\left(\frac{1}{2}\frac{dB}{dx}+\frac{h}{3}\frac{dm}{dx}\right) \tag{2.6}$$

where B is the bottom width of the channel, and m is the side slope of the trapezoidal channel.

For rectangular channels, $m = 0$, and I_1 and I_2 reduce to

$$I_1 = \frac{Ah}{2} \qquad I_2 = \frac{Ah}{2B}\frac{dB}{dx} \tag{2.7}$$

Substitution of equation (2.7) into (2.2) yields the conservative formulation for rectangular channel employed by Hicks and Steffler (1990):

$$\frac{\partial Q}{\partial t} + \frac{\partial}{\partial x}(QU) + \frac{\partial}{\partial x}\left(\frac{gAh}{2}\right) - \frac{gAh}{2B}\frac{dB}{dx} = gAS_o - gAS_f \tag{2.8}$$

where U= uniform cross-sectional velocity.

However, for natural channels, due to their irregular topography, direct integration of the term gI_2 in equation (2.2) can be problematic and difficult. The result is that it is not possible to manipulate the St. Venant equations for natural channels into a fully conservative formulation. However, Capart *et al.* (2003) proposed and alternative version of equation (2.2) which is suitable for manipulation into a fully conservative form, as discussed next.

For the same control volume as shown in Figure 2.1, assuming a relatively uniform velocity distribution (i.e. momentum correction coefficient, β, approximately equal to 1.0)

and a hydrostatic pressure distributions at a section, the integral horizontal momentum equation (per unit mass) :

$$\frac{\partial}{\partial t}\int_{x_1}^{x_2} Q + \left[\frac{Q^2}{A}\right]_{x_1}^{x_2} + \left[gI_1\right]_{x_1}^{x_2} + \frac{1}{\rho}\int_{\Gamma_o} pn_x d\Gamma_o + \frac{1}{\rho}\int_{\Gamma_o} \tau d\Gamma_o = 0 \qquad (2.9)$$

where x is the longitudinal coordinate, t is time, x_1 and x_2 are the left and right boundaries of the control volume, respectively, τ is the longitudinal component of the boundary shear stress, ρ is the density of water, p is the pressure, Γ_o is the wetted boundary surface, and n_x is the horizontal component of the unit vector outward normal to Γ_o

The third term in equation (2.9) represents the net pressure force acting on the downstream and upstream end sections of the control volume, while the fourth term represents the net longitudinal pressure acting on the control volume lateral and bottom boundaries. Taken together, these two terms represent the net pressure force acting on the water in the control volume. Evaluation of the end pressure terms using equation (2.3) is relatively straightforward for arbitrary cross-sections, as long as a table of widths as a function of elevation is available. Direct evaluation of the internal pressure term (the third term) can be problematic for arbitrary geometry because assumptions about the channel bathymetry between cross-sections must be made.

Capart *et al.* (2003) introduced a convenient approximation for the lateral and bottom pressure force term. Essentially, they made the approximation

$$\frac{1}{\rho}\int_{\Gamma_0} p n_x d\Gamma \approx \frac{1}{\rho}\int_{\Gamma_0} p_{\bar{H}} n_x d\Gamma \tag{2.10}$$

where the pressure p in the wetted boundary surface integral is approximated with a pressure, $p_{\bar{H}}$, which is calculated by assuming a constant water surface elevation, $\bar{H} = \frac{1}{2}(H_1 + H_2)$, over the control volume. In this investigation, instead of using $\bar{H} = \frac{1}{2}(H_1 + H_2)$, a formula is proposed to estimate $\bar{H}$ as follows:

$$\bar{H} = \alpha H_1 + (1-\alpha) H_2 \tag{2.11}$$

where H_1, H_2 are the water surface elevations at location x_1 and x_2, respectively, and α is a weighting coefficient, $0 \le \alpha \le 1$, which default to Capart *et al.*'s formula when α=0.5. Then, since the total hydrostatic pressure force acting on a control volume with a horizontal water surface is zero, the internal force can be calculated from the net force on the end sections as

$$\int_{\Gamma_0} p_{\bar{H}} n_x d\Gamma_0 = -\left[\rho g I_{1\bar{H}}\right]_{x_1}^{x_2} \tag{2.12}$$

where $I_{1\bar{H}}$ is calculated from

$$I_{1\bar{H}} = \int_{z_o}^{\bar{H}} (\bar{H} - z) b dz \tag{2.13}$$

With this approximation, the momentum conservation equation becomes

$$\frac{\partial}{\partial t}\int_{x_1}^{x_2} Q dx + \left[\frac{Q^2}{A}\right]_{x_1}^{x_2} + \left[g\left(I_1 - I_{1\bar{H}}\right)\right]_{x_1}^{x_2} = -\int_{x_1}^{x_2} gAS_f dx \qquad (2.14)$$

where the friction slope, S_f, has been introduced for the boundary shear stress term. In equation (2.13), the evaluation of the boundary pressure force along the control volume uses the same calculation procedure and data as the evaluation of the end pressure forces. In addition, the boundary pressure term has been converted from a source term to an apparent flux term, which may have numerical advantages.

2.2 Error Analysis

Clearly, the magnitude of the error introduced by the approximation in equation (2.10) depends on the water surface slope and the specific channel geometry. It is instructive to quantify the error for the simple case of a rectangular channel of varying width. An approximate method for evaluating the error in general cases (e.g. irregular shaped channels) is also suggested.

Consider a control volume of length Δx in a rectangular channel with bed slope S_o, divergent side wall slope S_B, and water surface slope S_W (shown in Figure 2.2). The actual pressure force acting on bottom boundary is

$$\frac{1}{\rho}\int_{\Gamma_o} pn_x d\Gamma = g\left[\left(H_1 - z_1\right)^2 S_B + \left(H_1 - z_1\right) S_o B_1\right]\Delta x$$
$$-\left[S_B\left(H_1 S_w + z_1 S_o - H_1 S_o - z_1 S_W\right) - S_B\left(H_1 - z_1\right) B_1 S_o + \frac{1}{2} B_1 S_o\left(S_W - S_o\right)\right]\Delta x^2 \quad (2.15)$$
$$+\left[\frac{1}{3} S_B {S_W}^2 - \frac{1}{6} S_B S_W S_o + S_B {S_o}^2\right]\Delta x^3$$

The approximate bottom boundary pressure force is

$$\frac{1}{\rho}\int_{\Gamma_o} p_{\bar{H}} n_x d\Gamma = g\left[\left(H_1 - z_1\right)^2 S_B + \left(H_1 - z_1\right) S_o B_1\right]\Delta x$$
$$-\left[S_B\left(H_1 S_W + z_1 S_o - H_1 S_o - z_1 S_W\right) - S_B\left(H_1 - z_1\right) B_1 S_o + \frac{1}{2} B_1 S_o\left(S_W - S_o\right)\right]\Delta x^2 \quad (2.16)$$
$$+\left[\frac{1}{4} S_B {S_W}^2 - \frac{1}{6} S_B S_W S_o + S_B {S_o}^2\right]\Delta x^3$$

where B_1 and z_1 is width of channel and bed elevation at location x_1, respectively.

The absolute error

$$\varepsilon = \int_{\Gamma_o} pn_x d\Gamma - \int_{\Gamma_o} p_{\bar{H}} n_x d\Gamma = \frac{1}{12}\rho g\left(\Delta x\right)^3 S_B S_W\left(S_W - 4S_o\right) \quad (2.17)$$

The relative error in the boundary pressure force term can be expressed by normalization using the maximum end pressure force

$$\varepsilon_p = \frac{\varepsilon}{P_{\max}} = \frac{\frac{1}{12}\rho g(\Delta x)^3 S_B S_W (S_W - 4S_o)}{\rho \frac{g}{2} B h^2} = \frac{1}{12}\left(\frac{\Delta B}{B}\right)\left(\frac{\Delta H}{h}\right)\left(\frac{\Delta H - 4\Delta Z}{h}\right) \quad (2.18)$$

where ε is absolute error, ε_p is relative error, $P_{\max}$ is the maximum end pressure force, $\Delta B = 2\Delta x S_B$, $\Delta H = \Delta x S_W$, and $\Delta Z = S_o \Delta x$. B and h are the width and depth of the channel (taken at the section with the greater total pressure force).

For a horizontal rectangular channel, $S_0 = 0$

$$\varepsilon = \frac{1}{12}\rho g(\Delta x)^3 S_B S_W{}^2 \quad (2.19)$$

and the relative error is

$$\varepsilon_p = \frac{\varepsilon}{P_{\max}} = \frac{\frac{1}{12}\rho \frac{g}{2} \triangle B(\triangle H)^2}{\rho \frac{g}{2} B h^2} = \frac{1}{12}\left(\frac{\triangle B}{B}\right)\left(\frac{\triangle H}{h}\right)^2 \quad (2.20)$$

As noted by Capart *et al.* (2003), the error vanishes when either the water surface is horizontal or the channel is prismatic and rectangular. The third power reduction in error with control volume length is also encouraging as this rate of convergence is better than the convergence rate for most numerical schemes commonly used for the St. Venant equations.

From equation (2.18), it is clear that the error will be relatively small for most situations. For example, if all three ratios on the right hand side of equation (2.18) are as large as 0.5, the relative error is about 1%. This suggests that the method would be accurate even for hydraulic jumps and steep surge waves.

For comparison, the error for Sanders (2001) approach is evaluated herein as well. As mentioned in the previous section, Sanders (2001) only considered the source term accounting for pressure caused by the varying width, hence only this term was compared. In Sanders approach, the pressure caused by the width variation is calculated using

$$\int_{\Gamma_S} p n_x d\Gamma_S = \rho g \bar{h}_c \Delta A \tag{2.21}$$

in which ΔA is the difference in flow area between the upstream and downstream ends of the control volume, using a constant depth (defined at the centre of the control volume), $\bar{h}_c$ represents the depth for the free surface to the centroid of this difference in area (Figure 2.3), and Γ_S is the side wall boundary (note that $\Gamma_S + \Gamma_B = \Gamma_o$, where Γ_B is the bed boundary. The error for the varying width pressure term introduced by equation (2.21) is then

$$\varepsilon_{S1} = -\frac{1}{12} \rho S_B \left(S_W - S_o \right)^2 \Delta x^3 \tag{2.22}$$

while the error introduced by Capart *et al.* (2003) approximation is

$$\varepsilon_{S2} = -\frac{1}{12}\rho S_B \left(S_W - S_o\right)^2 \Delta x^3 + \frac{1}{12}\rho S_B S_o{}^2 \Delta x^3 \tag{2.23}$$

Thus the difference in error associated with the sidewall pressure term approximations used by Sanders (2001) and Capart *et al.* (2003) is slight, only $\frac{1}{12}\rho S_B S_o{}^2 \Delta x^3$, and both approximations are equivalent for horizontal varying width channels (for which $S_o = 0$). It is also important to note that in the Capart *et al.* (2003) approximation, the two pressure source terms accounting for side wall and bed slope variation are converted to a flux term, resulting in a fully conservative formulation.

The preceding analysis for approximate equation in a rectangular channel provides general guidance but is not directly useful for general non-prismatic channel geometries. In such cases, an approximate error evaluation can be made by exploiting the third order convergence of the pressure approximation. Evaluating the pressure integral by subdividing the control volume into two halves, each with its own average water surface elevation, provides a more accurate estimation, even if the cross sectional information at the control volume midpoint is interpolated from the ends of the control volume. The difference between the single and double control volume estimates then provides a good estimate of the error in the original evaluation. For example, returning to the rectangular channel of varying width with the added condition of equal bed and water surface slopes, the error estimated by this procedure can be shown to be three quarters of the exact error.

The approximate error can then be used as a criterion for refinement of the spatial discretization.

2.3 Energy Loss

As implied above, the proposed formulation introduced an approximation for the pressure acting on the wetted boundary surface by assuming a constant water surface $\bar{H}$, which is calculated using formula (2.11) . (reproduced here for convenience)

$$\bar{H} = \alpha H_1 + (1-\alpha) H_2 \tag{2.11}$$

Therefore, is also desirable to evaluate the energy loss for the approximate equation, so as to determine the appropriate value of the weighting factor α to be used in equation (2.11). Since expansion and contraction in cross section is the common case of energy loss, for simplicity, considering a horizontal sudden expansion in width in rectangular channel without friction shown in Figure 2.4, theoretically, the head loss is obtained with Borda formula (Henderson 1966):

$$h_f = K\left(\frac{V_1}{2g} - \frac{V_2}{2g}\right)^2 \tag{2.24}$$

where h_f is the local head loss, V_1, V_2 is the velocity at section 1 and 2, respectively, and K is the local loss coefficient, usually is taken as 1.

Referring to Figure 2.4, the momentum equation is written as

$$\rho Q(V_2 - V_1) = P_1 + P' - P_2 \tag{2.25}$$

in which, P_1, P_2 is the pressure force at section 1and 2, respectively, P' is the pressure force at side wall, which is calculated in terms of $\bar{H}$

$$P' = \frac{1}{2}\rho g\left(B_2 - B_1\right)\bar{H}^2 \tag{2.26}$$

in which, B_1, B_2 is the width at section 1 and 2, respectively.

Based on equations (2.25), (2.26), (2.11) and the energy equation, it is obvious that the local loss coefficient varies depending upon the value of α used. This variation is illustrated in Figure 2.5 (a), for an upstream Froude number, F_1 , of 0.2, for both a sudden expansion ($B_2/B_1 > 1$) and a sudden contraction ($B_2/B_1 < 1$). For the sudden expansion, it is seen that the choice of α = 0.5 (Capart *et al.* 2003 approximation) is quite different from the Borda loss (K = 1). Furthermore, this choice produces a negative loss coefficient (energy gain) for the sudden contraction, which is physically unrealistic. Based on Figure 2.5 (a), it would seem that a value of α = 1.0 provides the best approximation to the Borda loss at this Froude number. Figure 2.5 (b) presents the variation in K for F_1 = 0.565, where the same tendency is seen. Thus, for sudden

expansions and contractions, a value of $\alpha = 1.0$ seems most appropriate (i.e. the upstream depth should be used as the constant depth in the approximation, not the average depth). However, in natural channels both gradual and sudden transitions in width may occur, and for the latter, a reduced loss coefficient would be expected. Hence, value of α ranging from 0.5 to 1.0 are likely appropriate for natural channels. However, larger values are indicated for contractions to avoid negative (i.e physically unrealistic) losses.

2.4 CDG Finite Element Implementation

In equation (2.14), the boundary pressure force apparent flux term is not continuous across the boundary between the two control volumes, since it is evaluated with different depths in each adjoining control volume. This consideration requires modifications to the usual finite element procedure for discretizing the St. Venant equations. The Characteristic-Dissipative-Galerkin procedure of Hicks and Steffler (1990) is considered in the subsequent analysis but the modification is general to any finite element method.

The differential equation that corresponds to equation (2.14) is

$$\frac{\partial Q}{\partial t} + \frac{\partial}{\partial x}\left(\frac{Q^2}{A} + g\left(I_1 - I_{1\bar{H}}\right)\right) = -gAS_f \tag{2.27}$$

with the provision that equation (2.27) does not apply at the nodes (taken to be the endpoints of the finite elements) where $\bar{H}$ changes discontinuously.

A Petrov-Galerkin weak statement for the differential form of equation (2.1) and equation (2.27) can be constructed by assembling weighted integrals over all of the finite elements in the domain:

$$\sum_{e=1}^{N_e} \int_e \begin{bmatrix} \mathbf{N}_i \left(\frac{\partial \mathbf{\Phi}}{\partial t} + \frac{\partial \mathbf{F}}{\partial x} + \mathbf{G}_c \right) \\ -\omega \frac{\Delta x}{2} \mathbf{W} \frac{d\mathbf{N}_i}{dx} \left(\frac{\partial \mathbf{\Phi}}{\partial t} + \mathbf{A} \frac{\partial \mathbf{\Phi}}{\partial x} + \mathbf{G}_n \right) \end{bmatrix} dx = \mathbf{0} \tag{2.28}$$

where

$$\mathbf{\Phi} = \begin{bmatrix} A \\ Q \end{bmatrix} \qquad \mathbf{F} = \begin{bmatrix} Q \\ \frac{Q^2}{A} + g\left(I_1 - I_{1\bar{H}}\right) \end{bmatrix}$$
$$\mathbf{G}_c = \begin{bmatrix} 0 \\ gAS_f \end{bmatrix} \qquad \mathbf{N}_i = \begin{bmatrix} f_i & 0 \\ 0 & f_i \end{bmatrix} \tag{2.29}$$

f_i is the finite element local interpolation (basis) functions, ω is the upwinding coefficient, usually set to 0.5 (Hicks and Steffler, 1992), and $\mathbf{W}$ is upwinding matrix.

The second term in equation (2.28) is the upwinding term and is based on the non-conservative form of the St. Venant equations with the convection matrix

$$\mathbf{A} = \frac{\partial \mathbf{F}}{\partial x} = \begin{bmatrix} 0 & 1 \\ -U^2 & 2U \end{bmatrix} \tag{2.30}$$

where U is the average channel velocity ($U = Q/A$).

The source terms for the non-conservative form are

$$\mathbf{G}_{\mathbf{n}} = \begin{bmatrix} 0 \\ g\dfrac{\partial}{\partial x}\left(I_1 - I_{1\bar{H}}\right) + gAS_f \end{bmatrix} \tag{2.31}$$

Integration by parts of the flux derivative in equation (2.28) yields

$$\sum_{e=1}^{N_e} \int_e \begin{bmatrix} \mathbf{N}_i \dfrac{\partial \mathbf{\Phi}}{\partial t} - \dfrac{\partial \mathbf{N}_i}{\partial x}\mathbf{F} + \mathbf{N}_i \mathbf{G}_{\mathbf{c}} \\ -\omega \dfrac{\Delta x}{2} \mathbf{W} \dfrac{d\mathbf{N}_i}{dx}\left(\dfrac{\partial \mathbf{\Phi}}{\partial t} + \mathbf{A}\dfrac{\partial \mathbf{\Phi}}{\partial x} + \mathbf{G}_{\mathbf{n}}\right) \end{bmatrix} dx + \sum_{e=1}^{N_e} \left(\mathbf{N}_i \mathbf{F}\right)\Big|_{l_e}^{r_e} = \mathbf{0} \tag{2.32}$$

which, as a weak form of equation (2.27), admits discontinuous solutions. The element boundary flux terms are

$$\left(\mathbf{N}_i \mathbf{F}\right)\Big|_{l_e}^{r_e} = \begin{bmatrix} f_i Q \\ f_i\left(QU + gI_1 - gI_{1\bar{H}}\right) \end{bmatrix}\Bigg|_{l_e}^{r_e} \tag{2.33}$$

where l_e and r_e represent the left and right boundary location of each element e, respectively. Normally the flux contributions from adjoining elements offset each other on all inter-element boundaries, leaving only the flux contributions at the domain boundaries. However, in this formulation, $I_{\bar{H}}$ is discontinuous across inter-element boundaries since the average elevation used changes discontinuously from element to element. Therefore, the boundary flux term must be evaluated as

$$\sum_{e=1}^{N_e} \left(\mathbf{N}_i\mathbf{F}\right)\Big|_{l_e}^{r_e} = \sum_{e=1}^{N_e} \left[\begin{matrix} 0 \\ f_i\left(-gI_{1\bar{H}}\right)\end{matrix}\right]\Bigg|_{l_e}^{r_e} + \left[\begin{matrix} f_iQ \\ f_i\left(QU + gI_1\right)\end{matrix}\right]\Bigg|_0^L \tag{2.34}$$

where 0 and L denote the boundaries of the domain.

With the additional inter-element contributions in equation (2.34), the global matrices can be assembled as usual (Hicks and Steffler, 1990). A variably implicit finite difference time stepping scheme is used to develop the final set of non-linear discrete algebraic equations and a Newton-Raphson iterative method is used to solve them at each time step. Details of the implementation of the CDG finite element scheme are provided in the Appendix A.

2.5 Discretization

Discretization is related to the accuracy and stability of the numerical scheme. Two factors to consider in discretization are the time step increment and the spatial

discretization. Typically these two are closely tied, related to each other through the commonly know *Courant condition*:

$$C = \frac{V_w \ \Delta t}{\Delta x} \tag{2.35}$$

where, C is the Courant number, V_w is the wave speed, Δt is the time step increment, and Δx is the distance between computational nodes. The required Courant number is dependent upon the numerical scheme employed, and has significant implications for ensuring solution accuracy (and sometimes stability, as well). For the finite element scheme employed in the *RIVER1D* model, typically a Courant number of 0.5 or less is recommended for dynamic problems, with solution accuracy increasing with decreasing Courant number.

Typically, this Courant number requirement is a strict issue for dynamic (acceleration dominated) waves only. In the case of modeling diffusive (friction dominated) waves, such as encountered in the typical open water flood routing situation, quite often good solution accuracy can be achieved at significantly higher Courant numbers (with implicit models such as these), because the length of the wave being modeled is typically quite large compared to the flow depth (Hicks and Steffler 199). For example, in the original application of the *cdg1-D* (RIVER1D precursor) model for the Oldman River, AB (McKay *et al.*, 1996), using a rectangular channel approximation throughout with a

section spacing of 1 km, it was found that a time step increment of up to 1h could be employed without loss of accuracy ($C \sim 15$).

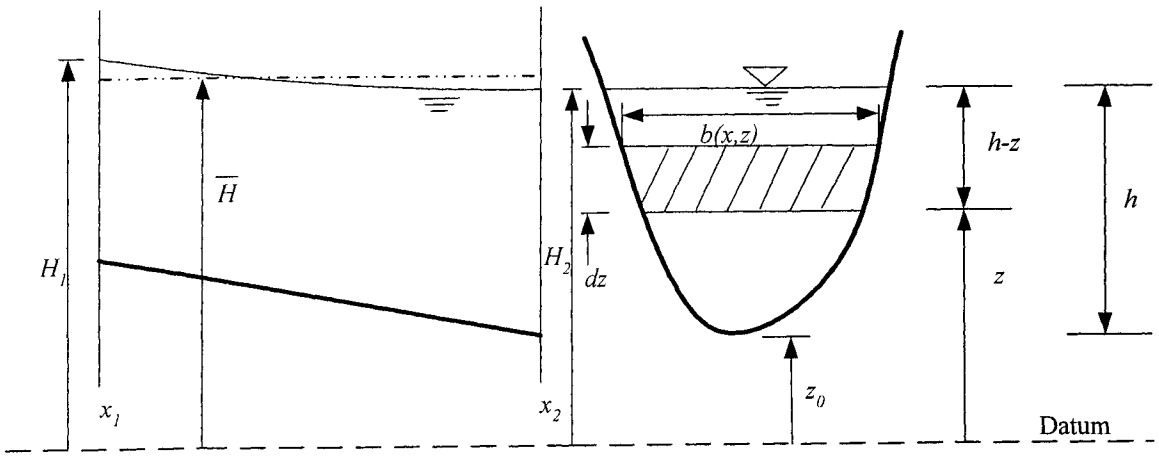

Figure 2.1 Control volume for 1-D open channel flow (adapted from Capart *et al.* 2003).

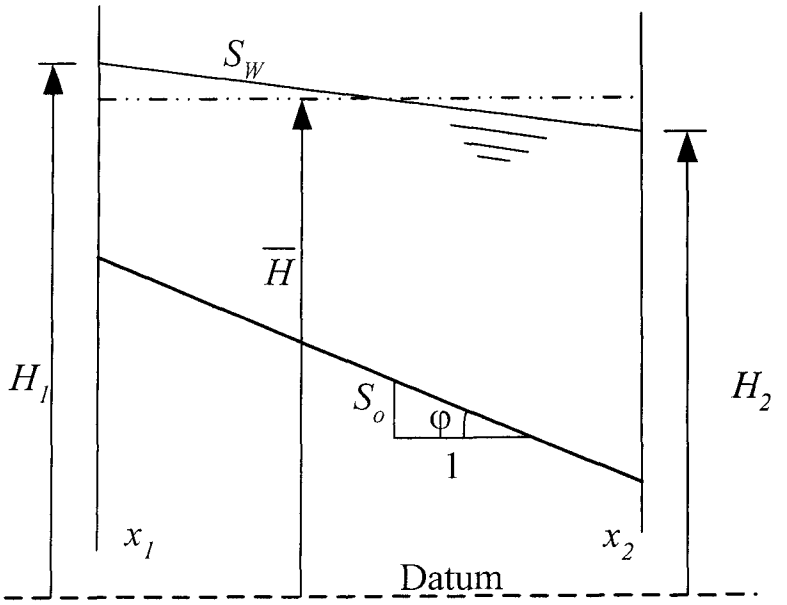

(a)

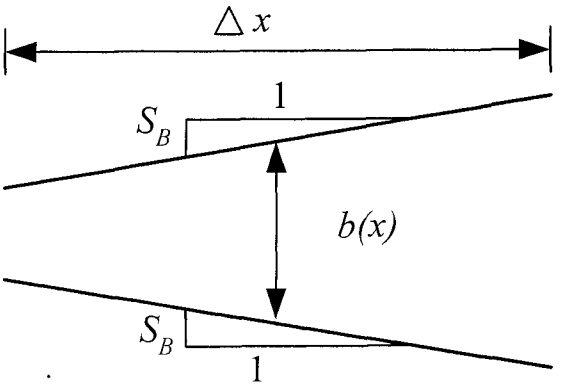

(b)

Figure 2.2 Definition sketch of an expanding rectangular channel.
(a) Profile; (b) Plan view.

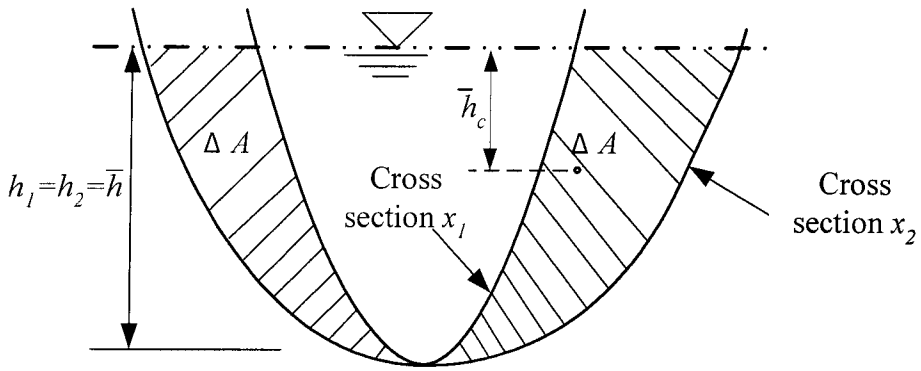

Figure 2.3 Calculated definition sketch in Sanders' approach (2001).

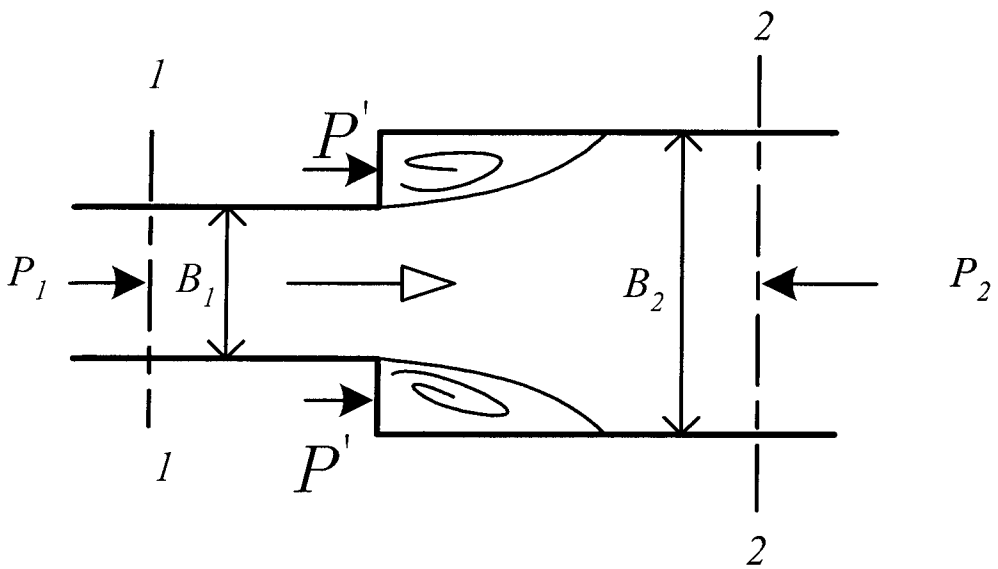

Figure 2.4 Plan view of abrupt expansion.

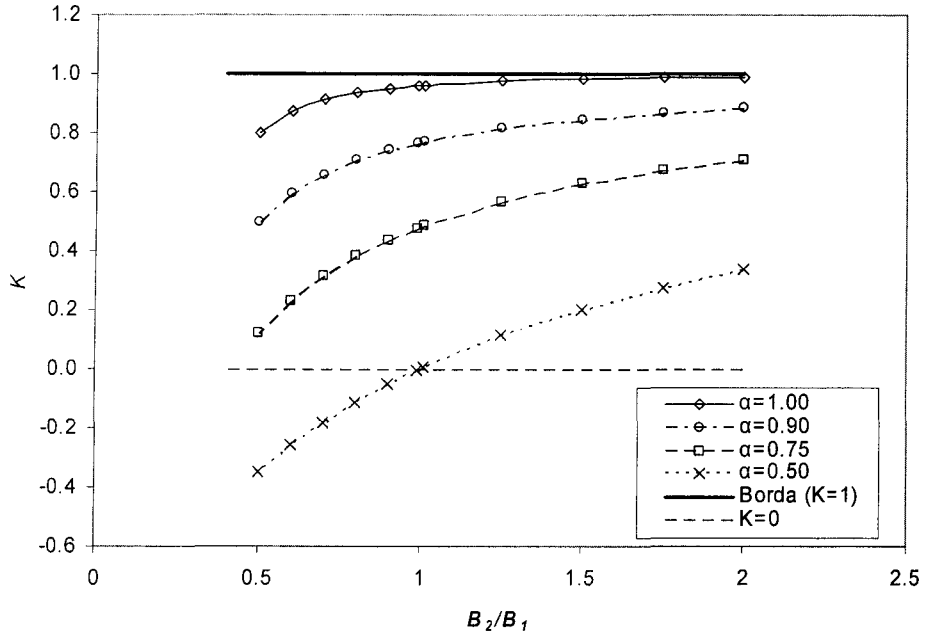

(a) (F_1=0.2, Q=1.5 m^3/s, B_1=1m, h_1=1.79m).

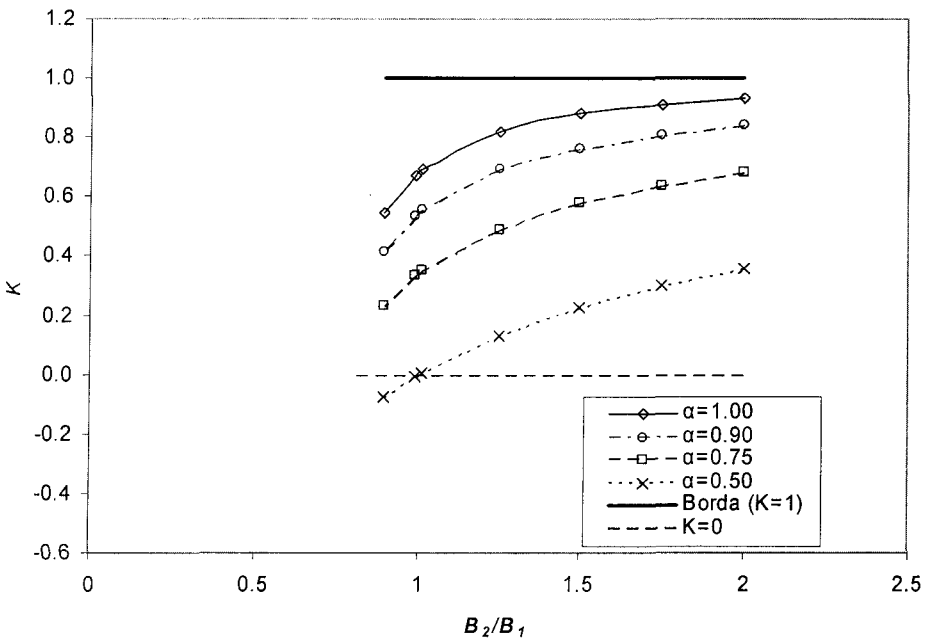

(b) (F_1=0.565, Q=5 m^3/s, B_1=1m, h_1=2m).

Figure 2.5 Comparison of local loss coefficient K.

CHAPTER 3

MODEL VALIDATION

3.1 Introduction

Four numerical tests were conducted herein to validate the numerical scheme, involving both steady and unsteady flow tests. The results obtained using the approximate St.Venant equation are also compared to those obtained by other investigators and to experimental data. For steady flow, first, the transition at two slope bed was considered; then the model was applied to the same steady flow problem tested by Capart *et al.* (2003) (hydraulic jump in an expanding channel) to validate the numerical scheme used herein, and to quantify the error associated with the approximate formulation. The unsteady flow tests included the classical dam break in a prismatic channel as well as a dam break in a converging and expanding channel, with comparison of the latter results to the experiment data of Bellos *et al.* (1992).

3.2 Steady Flow Simulation

3.2.1 Transition from mild to steep slope

One of the attractive properties of the finite element method is that separate algorithms are not required for the transition between supercritical and subcritical flow. The transition from a mild to a steep sloped channel is one challenging test of this capability

employed earlier by Hicks and Steffler (1990). The behavior of the proposed approximate formulation is first checked for this case.

Upstream and downstream slopes in a 10m wide, 650m long rectangular channel are taken as 0.0025 and 0.04, respectively. The effective bed roughness is set to 0.2m. Accordingly, for a steady discharge of $100m^3/s$, the flow in upstream and downstream segments corresponds to subcritical and supercritical flow, respectively. The domain is discretized into 65 elements each 10m long. Initial conditions for the test are: flow depth of 3.5 and discharge of $100m^3/s$ in entire domain. Normally two boundary conditions are required to solve open channel flow problems, one upstream and one downstream (subcritical flow) or two upstream (supercritical flow). However, this is a unique problem since the flow in the upstream half of the domain is subcritical whereas the flow in the downstream half is superctitical. Thus, technically, only a single upstream boundary condition is needed (typically a specified flow). This is, in part, what makes this a channeling numerical problem.

The unsteady flow routine was used as a means to solve for this steady problem, by inputting an arbitrary initial condition for the depths throughout the domain and then running the model until a steady state solution was achieved. Figure3.1 presents the numerical results using an upwinding coefficient, ω, of 0.5 and a time step increment of 0.5s, which corresponds to a Courant number of about 0.35. These results are nearly identical to Hicks and Steffler (1990), with only a slight local oscillation evident at the slope break. The maximum discharge error at the slope break is 0.129% for the

approximate equation, compared to 0.042% for Hicks and Steffler (1990) for the exact equation.

3.2.2 Hydraulic jump in an expanding channel

As shown in Figure 3.2, the modeled channel has a horizontal bottom and a rectangular cross section with a divergent sidewall, expanding from an upstream width of 0.155 m to a downstream width of 0.460 m. The channel is assumed to be frictionless. The flow scenario involves a steady discharge of 0.0263 m^3/s. At the upstream boundary (located at station 0.30 m) the depth was set to 0.088 m (supercritical flow) while the depth at the downstream boundary was set to 0.195 m (subcritical flow), to ensure that a hydraulic jump occurs in the channel.

The initial depth conditions within the domain were as follows: a depth of 0.088 m was specified from the upstream boundary to a location of x =1.1 m, and a depth of 0.195 m was specified from station x = 1.1 m to the downstream boundary. This places the jump initially in approximately the correct location. (Additional tests were conducted and it was found that the final steady state solution was not sensitive to the location of the jump as an initial condition.) The entire domain was discretized with 0.1m long elements. The time step increment was set to 0.01s, corresponding to a Courant number that is less than or equal to 0.5 (required to ensure solution stability in this particular case).

The computational results were compared to the experimental data obtained by Khalifa (1980) and were in good agreement, particularly in terms of the location of hydraulic

jump (Figure 3.3). For comparison purposes, these results are also compared to those obtained by Younus and Chaudhry (1994) using a 2-D depth-averaged k-ε turbulence model, and to those obtained by Capart *et al.* (2003) using a finite volume approach. Clearly the current model performs well in comparison, albeit with small oscillations in the vicinity of the jump. Khan and Steffler (1995) have demonstrated that the finite element model's performance in the vicinity of hydraulic jumps, both in terms of sensitivity to discretization and local oscillation, is improved by adding a momentum flux term to the momentum equation, related to the non-uniform velocity distribution and turbulent stress.

Employing equation (2.18) to quantify the error associated with the approximate formulation for this problem, it was determined that the maximum percent error, ε_p was only 0.34%. This demonstrates that this approximate conservative formulation is quite valid for this situation, despite the significant sidewall inclination and steep water surface slope associated with the hydraulic jump.

3.3 Unsteady Flow Simulation

To demonstrate the approximate formulation's performance for shock capturing, two unsteady flow tests were conducted, including a classic dam break problem in a rectangular channel, for both constant and varying width scenarios.

3.3.1 Dam break in prismatic rectangular channel

Numerous test cases have been developed for an ideal instantaneous failure of dam in a frictionless, horizontal, prismatic, rectangular channel (Fennema and Chaudhry 1987; Fread 1988; Hicks and Steffler 1990). For this simulation, the test of Hicks and Steffler (1990) is reproduced. It involves a unit width channel (i.e. 1 m wide), consisting of 80 elements each having length of 25 m. A zero initial discharge is set to for entire domain. The boundary conditions are specified as zero discharge at both ends. The initial flow depth is 10m for the upstream half, whereas for the downstream half, two possible depths are considered. One is 5 m (h_d/h_u=0.5), the other is 0.5 m (h_d/h_u =0.05).

Figure 3.4 shows the initial conditions and result for the first test in which $h_d/h_u = 0.5$. The maximum time step to obtain a stable solution is 1.25 s, corresponding to a Courant number of 0.46. Comparison of the computed results to the analytical solution (Hicks and Steffler, 1990) shows good agreement. The shock spreads over three elements and only small pre- and post-shock oscillations are observed for the progressive wave. Only minor damping of the regressive wave is evident.

The result for the second test case, in which $h_d/h_u = 0.05$, is presented in Figure 3.5. This was a much more challenging test case because of the small downstream water depth. The situation can lead to negative depths in the solution if there are depth oscillations, which is likely to lead to the solution failure. Consequently, the model had to be run at the time step increment of 0.625 s to obtain a stable solution. This corresponds to a Courant number of 0.25. The simulation result illustrates that the proposed formulation is

stable and reasonably accurate, although there are trailing disturbances appearing for the progressive wave. Again the regressive wave shows only minor damping.

3.3.2 Dam break in a converging and diverging channel

The approximate conservative formulation was further evaluated for the propagation of a dam break surge wave in a converging and diverging rectangular channel, with comparison to the experimental results of Bellos *et al.* (1992). Figure 3.6 shows the plan view of their experimental setup. The channel was rectangular, with a maximum width of 1.4m gradually narrowing to 0.6m over a 3.5m length; it then expanded back out to 1.4m over the next 8.0m of length. A gate, acting as the dam, was fixed at the location of minimum width (x=8.5 m). Water levels were monitored at 5 stations along the centerline of flume, as indicated in Figure 3.6.

Because the experimental flume had a gate at the downstream end, the propagating surge reflected back up the channel during the experiments. However, the details of this end gate configuration were not available, so the computational domain was extended to eliminate the effect of the downstream boundary in the numerical simulation. Each element was 0.5 m in length and the time step increment was taken as 0.1s. For the initial conditions, a zero discharge was set throughout domain which means the velocity is zero; the flow depth upstream of the gate was set to 0.20 m and that downstream of the gate to 0.101 m as was the case in the corresponding experiment. The upstream and downstream boundary conditions were both specified as a zero discharge. Manning's coefficient was set to 0.012 (as suggested by Bellos *et al.*, 1992).

Figure 3.7 presents a comparison of the water levels obtained with the numerical model to the experimental data at 5 different locations where it is seen that the predicted values are in good agreement with the experimental data. It should be noted that the numerical results differ from the experimental measurements near the end of the simulation at locations 13.5 m and 18.5 m, as the reflected wave in the flume was not modeled in this simulation. Again, employing equation (2.18), the maximum error was found to be 0.0064%, which is negligible. Similarly good results were obtained for other ratios of upstream and downstream water depth, also comparing to Bellos *et al.*'s (1992) data (see Figure3.8 to 3.10). This demonstrates the validity of Capart *et al.*'s (2003) approximate conservative formulation.

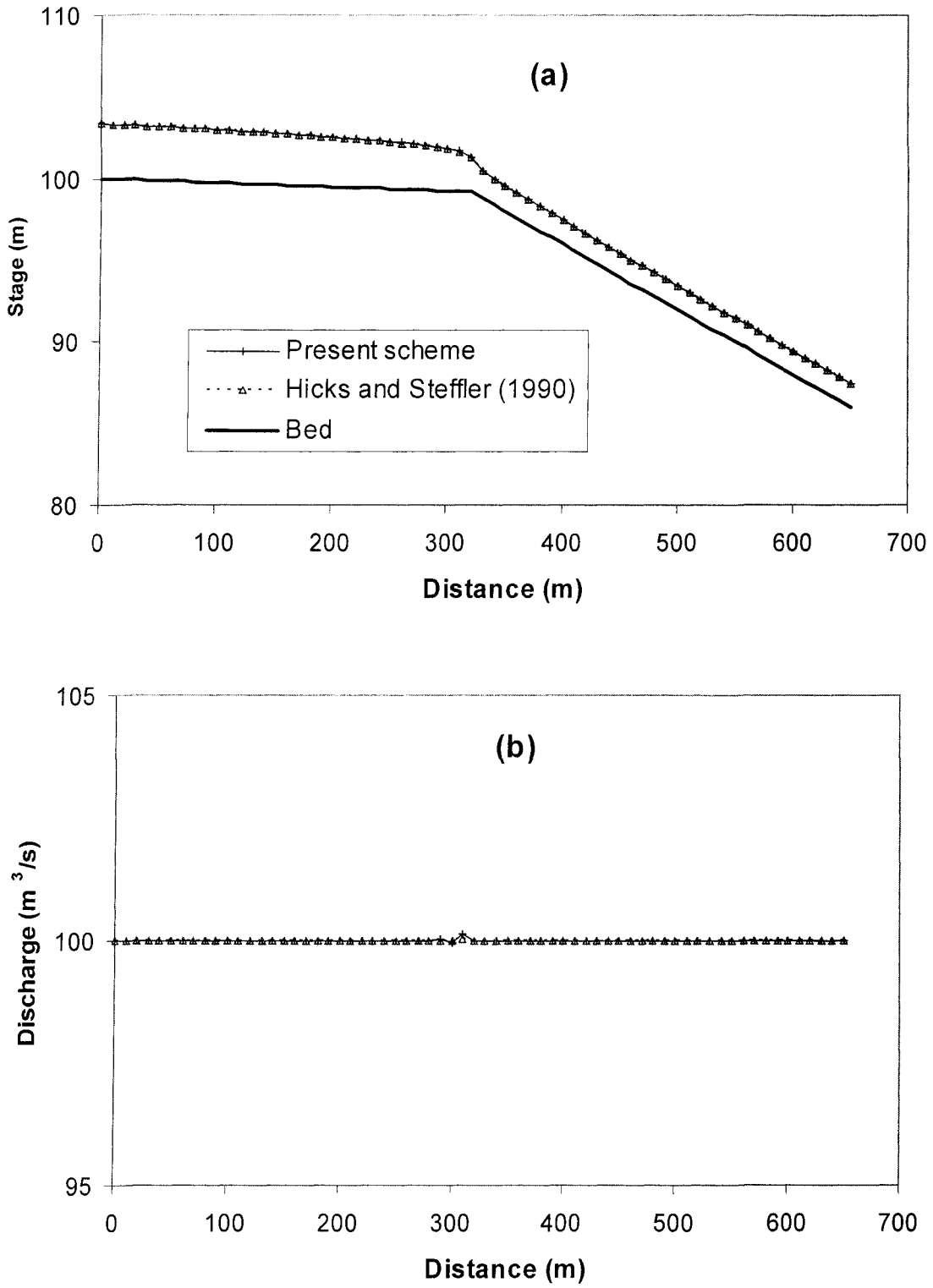

Figure 3.1 Transition from mild to steep slope. (a) Stage; (b) Discharge (ω=0.5, Δt=0.5s).

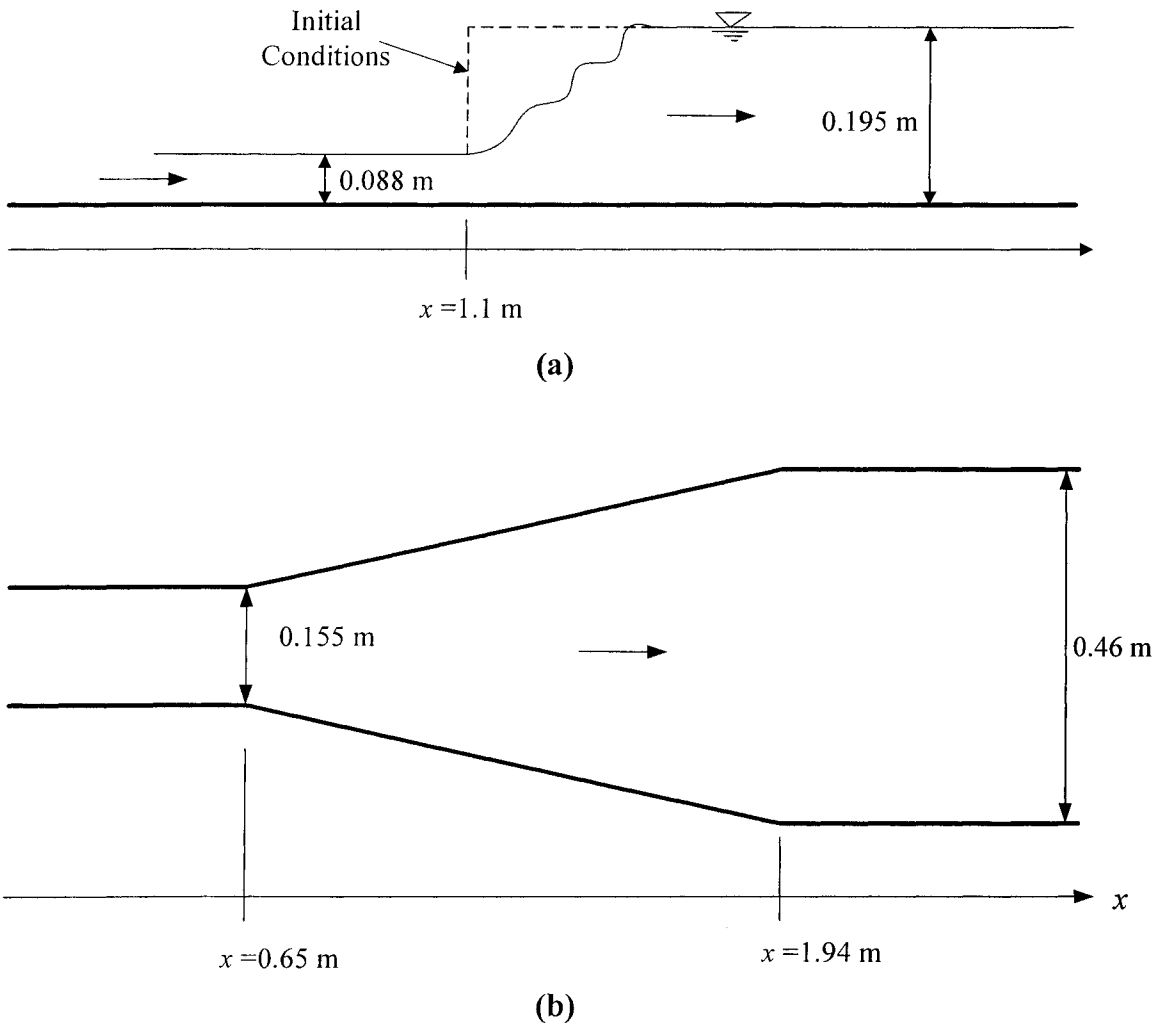

Figure 3.2 Schematic diagram of hydraulic jump in an expanding channel.
(a) Longitudinal section; (b) Plan view. (adapted from Younus and Chaudhry, 1994).

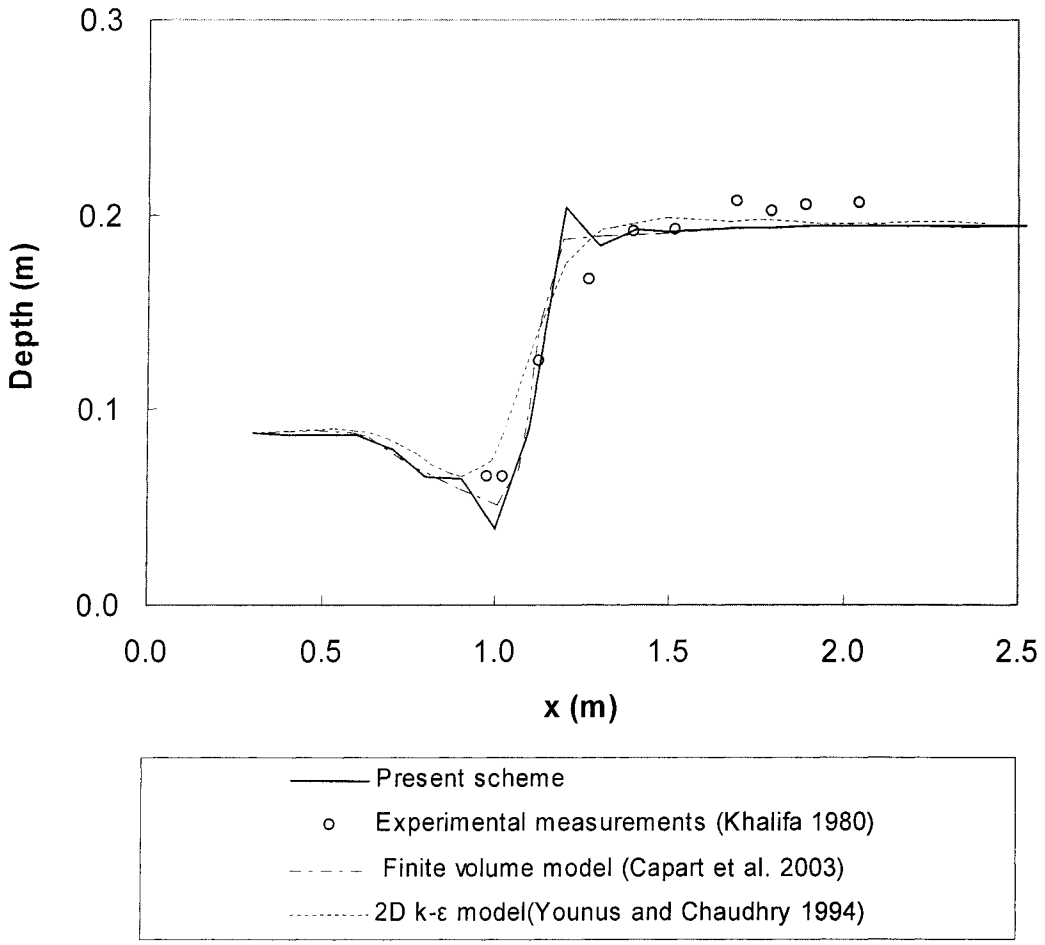

Figure 3.3 Comparison of computed and observed values for the centerline profile of a hydraulic jump in expanding channel.

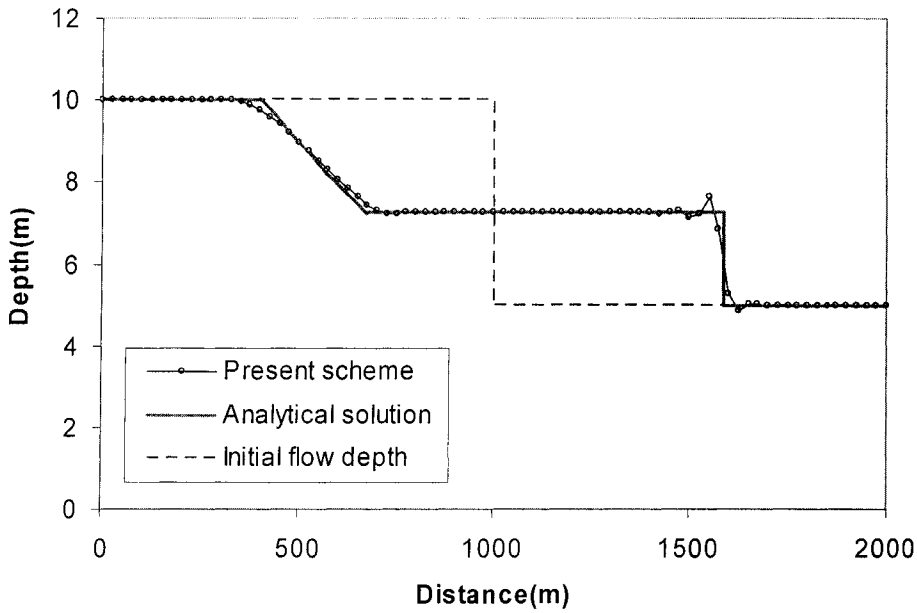

Figure 3.4 Numerical solution for dam break.
(H_d/H_u=0.5, t=60s, θ=0.5, ω=0.25, Δt=0.625s).

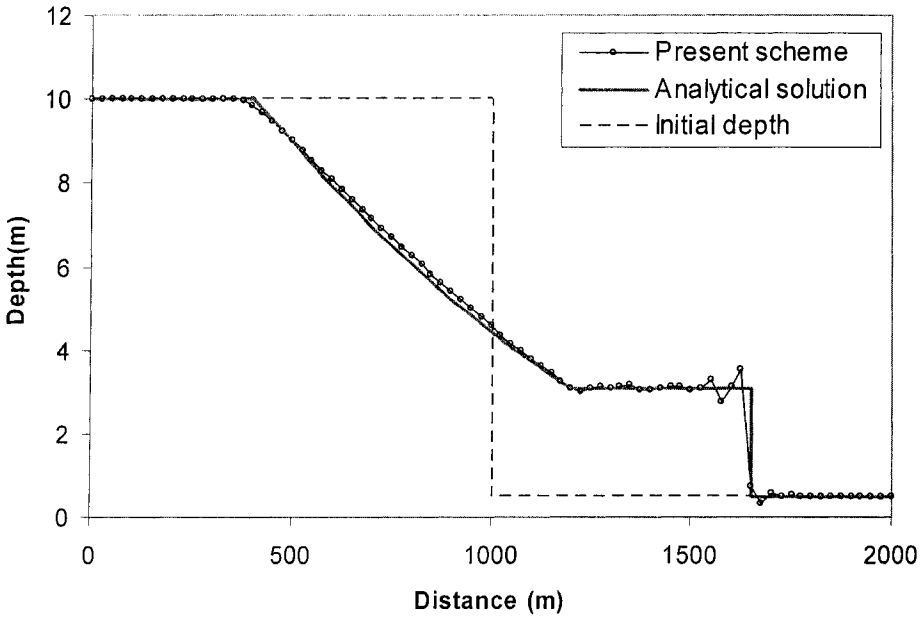

Figure 3.5 Numerical solution for dam break.
(H_d/H_u =0.05, t=60s, θ=0.5, ω=0.25, Δt=0.625s).

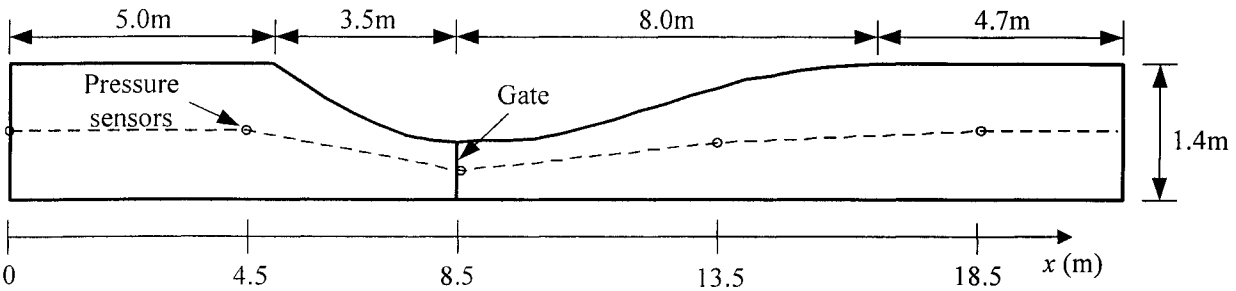

x axis label, distance from upstream boundary (m)

Figure 3.6 Plan view of experimental setup used by Bellos *et al.*.(1992).

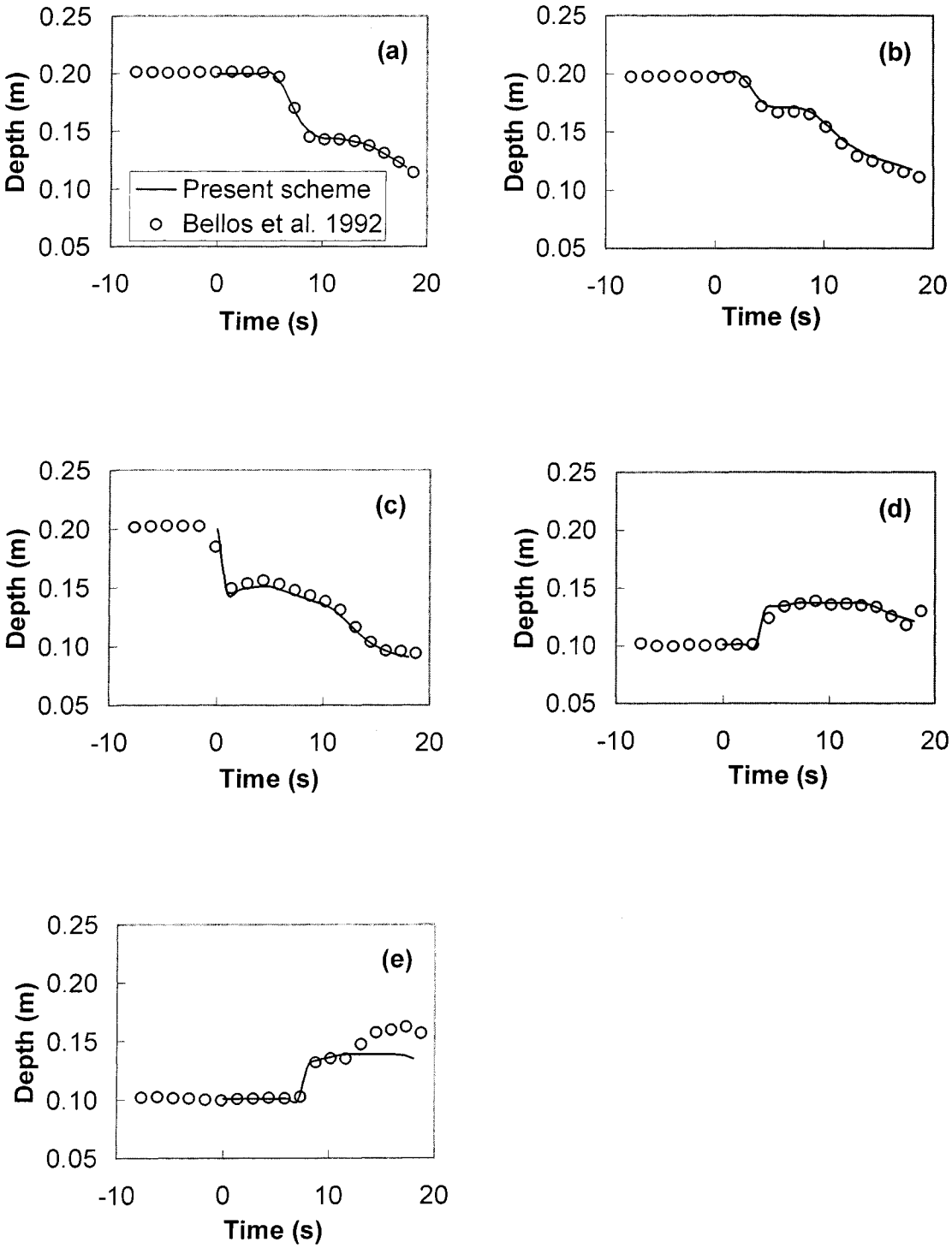

Figure 3.7 Comparison of numerical results with experimental data for h_u/h_d =2.0. (a) x=0.0m; (b) x=4.5m; (c) x=8.5m; (d) x=13.5m; (e) x=18.5m.

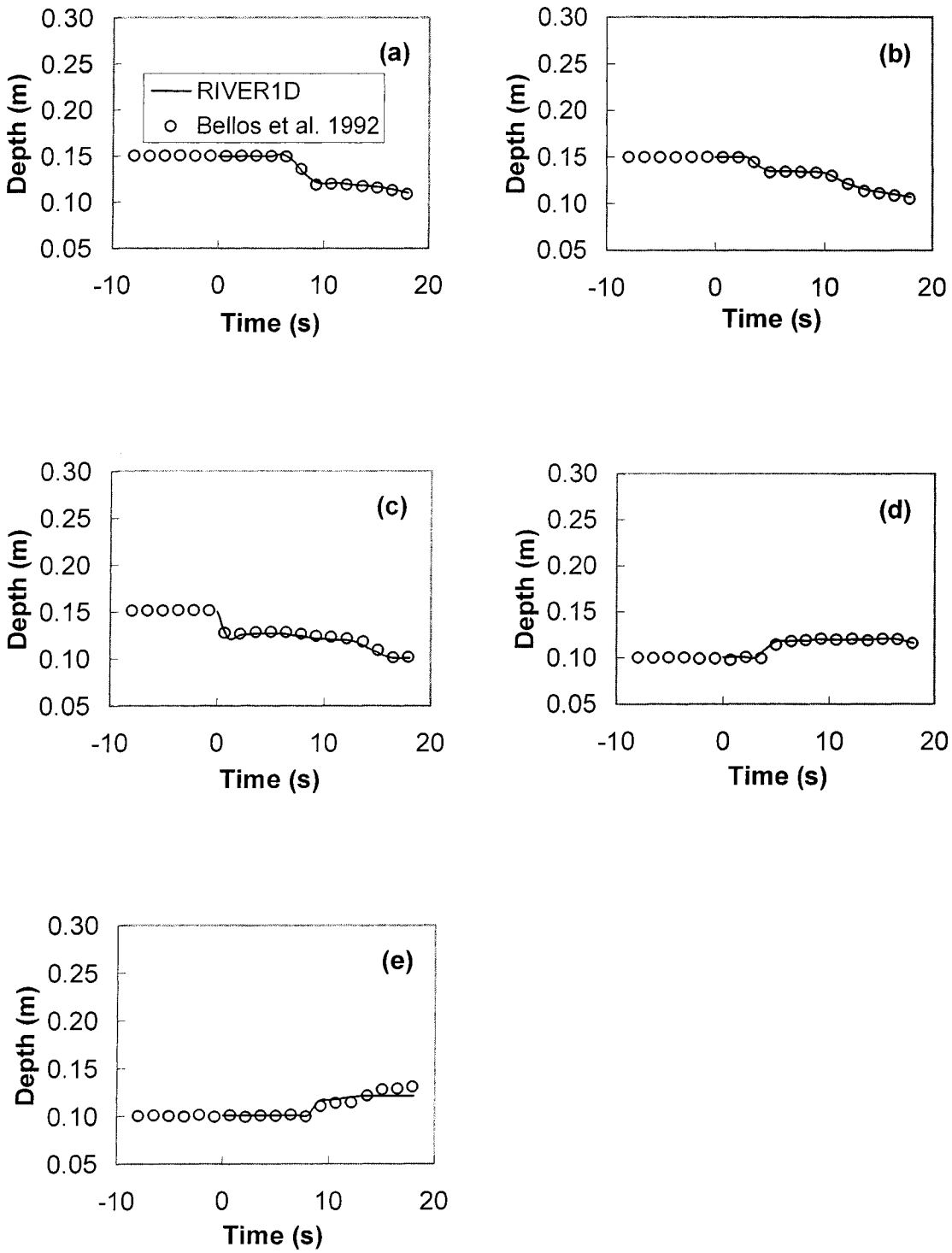

Figure 3.8 Comparison of numerical results with experimental data for h_u/h_d =1.5. (a) x=0.0m; (b) x=4.5m; (c) x=8.5m; (d) x=13.5m; (e) x=18.5m.

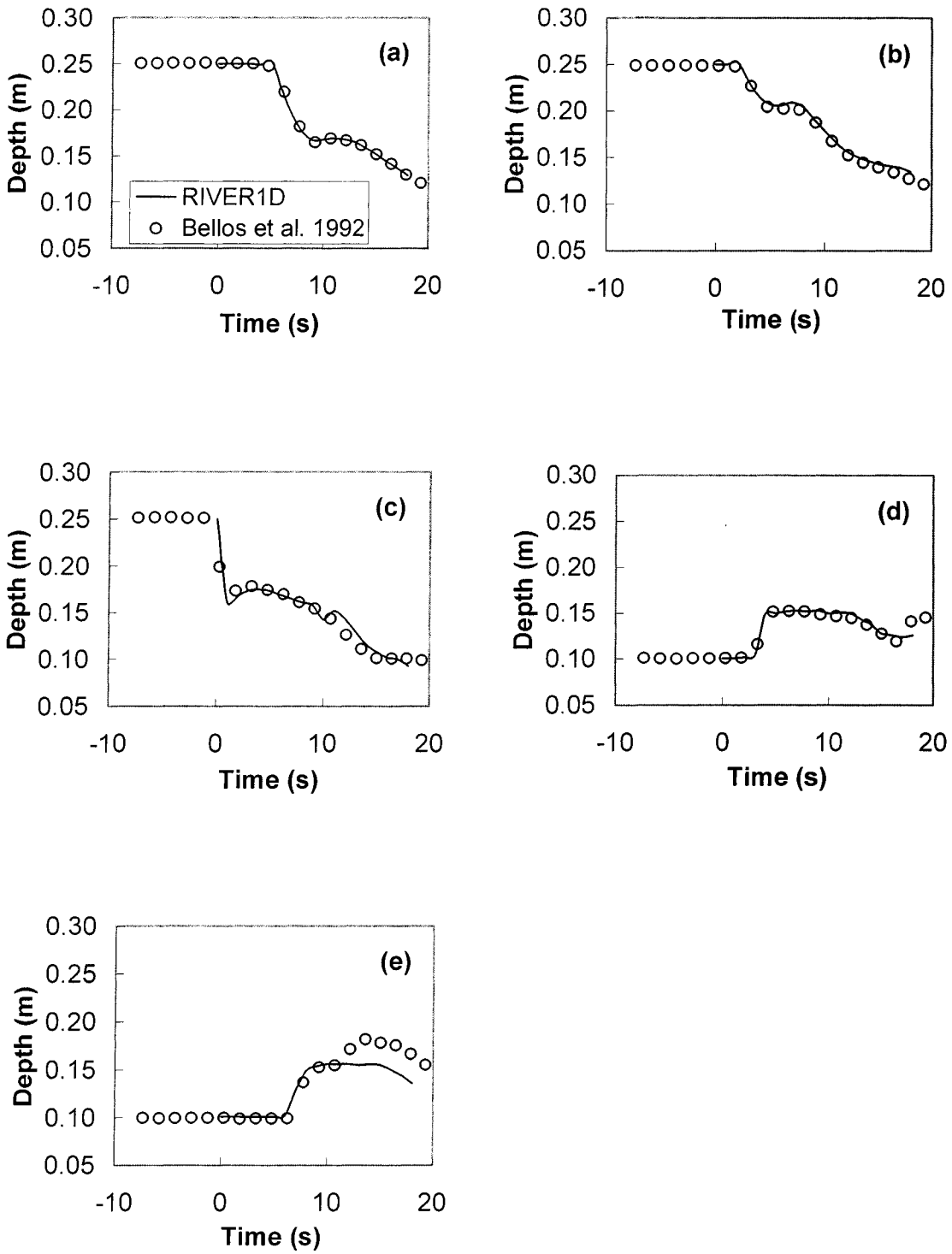

Figure 3.9 Comparison of numerical results with experimental data for h_u/h_d =2.5. (a) x=0.0m; (b) x=4.5m; (c) x=8.5m; (d) x=13.5m; (e) x=18.5m.

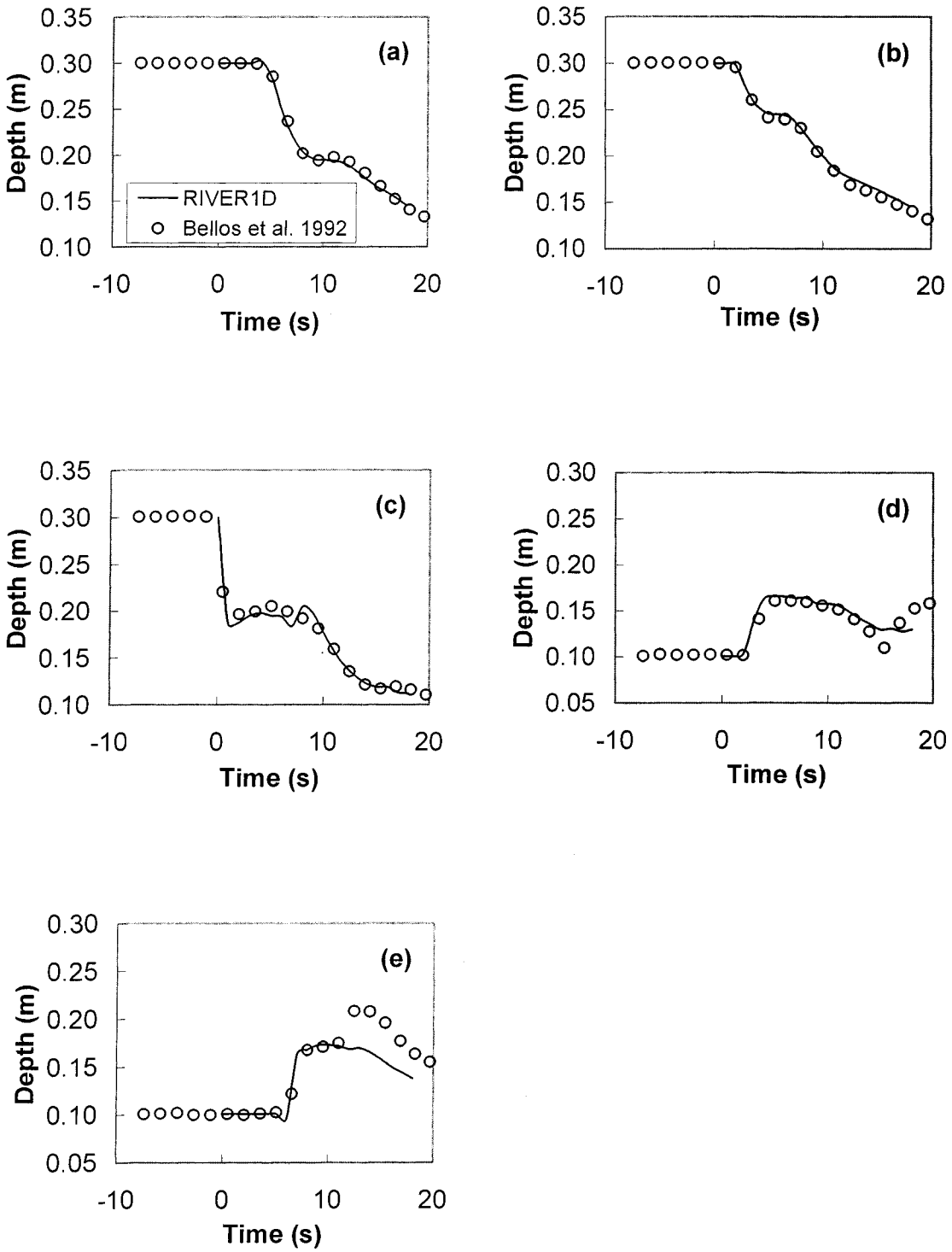

Figure 3.10 Comparison of numerical results with experimental data for h_u/h_d =3.0. (a) x=0.0m; (b) x=4.5m; (c) x=8.5m; (d) x=13.5m; (e) x=18.5m.

CHAPTER 4

MODEL APPLICATION

-FLOOD ROUTING IN OLDMAN RIVER

4.1 Overview

A key purpose motivating the development of the approximate conservative formulation is its application in natural channels. To investigate the applicability and reliability of the approximate formulation for a real river, the 1995 flood event in the Oldman/South Saskatchewan River in southern Alberta was simulated using the new RIVER1D.

Figure 4.1 illustrates the Oldman\South Saskatchewan River basin in southern Alberta. The reach modeled for this investigation extends from the Oldman Dam, through the communities of Fort McLeod and Lethbridge and downstream to the confluence with the Bow River, where the two rivers combine to form the South Saskatchewan River. The modeled reach further extends downstream past the community of Medicine Hat a distance of 20 km.

In 1995 a major flood occurred in the Oldman River basin, and although the Oldman Dam was successful in mitigating the event to some extent, a 1:100 year flood was still experienced downstream on the Oldman and South Saskatchewan Rivers. McKay *et al.* (1996) illustrated the application of hydraulic flood routing for that event, by employing a rectangular approximation for the channel geometry. They used the precursor to the

RIVER1D model (known at the time as the *cdg1-D* model) which employs the same finite element scheme applied to the simpler equation formulation (2.8), limited in applicability to rectangular channels. The flood routing conducted for that investigation was limited to the reach extending from Lethbridge to Medicine Hat, because of insufficient data on tributary inflows upstream. It was found that the *cdg1-D* hydraulic model provided good estimates of the flood peak magnitude and timing at Medicine Hat, and captured the overall shape of the flood hydrograph there. However, comparison to upstream stations could not be conducted because of the missing tributary data. Also, water levels were not accurately reproduced with the approximate geometry.

More recently, there have been additional geometric surveys of the Oldman River and these, in combination with earlier surveys at Fort Mcleod, Lethbridge and Medicine Hat, potentially provide sufficient data to create a 'combined geometry' hydraulic routing model of the Oldman/South Saskatchewan Rivers, similar to that developed for the Peace River in northern Alberta (Blackburn and Hicks 2002). Such a model would potentially have the capability of providing accurate predictions of both discharge and water level in flood forecasting applications. In addition, further details regarding tributary inflows have been obtained, facilitating the extension of the modeled reach.

4.1 Available Data

4.2.1 Channel geometry data

In the earlier study (McKay *et al.* 1996), river stations, or locations along the channel length, were established by marking out 1 km intervals on 1:50,000 scale National Topographic Series (NTS) maps, using a scale and dividers. The origin (station 0.0 km) was specified to be at the downstream face of the Oldman Dam, and river stations were specified in river km downstream of this origin. For simplicity, the stations were measured along the channel centerline, rather than along the thalweg, as the latter is somewhat subjectively determined when cross section data is limited.

Within this reach, there are four areas for which surveyed channel geometry data are available, specifically in a reach just downstream of the Oldman Dam (20 cross sections) and at the communities of Fort Mcleod (31 cross sections), Lethbridge (74 cross-sections), and Medicine Hat (64 cross-sections). Hicks *et al.* (2005) provide details of all these available cross section surveys, including cross section plots, the corresponding station and elevation data, and any known information on the sections' origin and date of survey. All of these cross sections were included in the hydraulic model, with the exception of those at Fort Mcleod, as all attempts to incorporate those were unsuccessful. Upon visual inspection of the cross section plots it became obvious that there are significant questions regarding the accuracy of these cross-sections, since much of the data looks unrealistic. Therefore, in order to complete working models of the river in *RIVER1D*, the natural cross sections at Fort Mcleod were ultimately omitted from the hydraulic model.

Figures 4.2 to 4.4 provide location maps for the remaining reaches containing natural cross sections. The cross-section locations shown in these maps were based on map and photo information provided by Alberta Environment. It should be noted that the locations of sections 14.1, 21.0 and 57.7 (shown in Figure 4.2 (a) and (b)) are estimated, since inadequate information was available with which to accurately locate them.

As done by *McKay et al.* (1996), between these communities the channel geometry in the hydraulic models was approximated by a simple rectangular shape, with the widths determined at 1 km intervals using 1:50,000 scale National Topographic Series (NTS) maps (McKay *et al.* 1996). The channel bed slope in these unsurveyed reaches was approximated from the water surface slopes obtained by identifying locations where topographic contours intersected the river channel on these same 1:50,000 scale NTS maps (McKay *et al.* 1996). Table 4.1 presents the water surface slopes obtained by the method. Figure 4.5 illustrates the resulting estimated bed profile used in the hydraulic model.

Table 4.1 Water surface slopes based on the NTS map data. (McKay *et al.* 1996)

Reach (km)	Water Surface Slope
169 to 205	0.001100
205 to 335	0.000725
335 to 550	0.000400

4.2.2 Channel Resistance Data

Channel resistance, specifically Manning's n, is the only calibration parameter required for this hydraulic flood routing model. In the context of a limited geometry model (i.e. for the routing reaches between communities) this must represent a composite resistance of both the channel and floodplain, including the effects of storage associated with floodplain inundation. Initially, a value of 0.030 was estimated for this parameter throughout all of the routing reaches, based on an average of channel roughness values reported by Kellerhals, Neill, and Bray (1972) for sites along the Oldman and South Saskatchewan Rivers.

For the sub-reaches where surveyed channel geometry was available from floodplain studies (Lethbridge and Medicine Hat) channel roughness was based on the HEC-2 data files from which the channel geometry data were obtained. Thus, they are based on values calibrated with a steady flow model for the corresponding floodplain studies.

4.2.3 Hydrologic Data

A key objective of this investigation was to illustrate (and evaluate) the model's performance for extreme events. The 1995 flood in southern Alberta provided the most extreme event documented, and so was ideal for this purpose. Water Survey of Canada (WSC) gauges operate within the study reaches at three sites; these are summarized in Table 4.2, along with their locations in km downstream of the Oldman Dam. The locations of these gauges are also indicated on the maps in Figures 4.2 to 4.4.

Table 4.2 Water Survey of Canada gauges on the Oldman and S. Sask. Rivers

WSC Gauge Name	Number	Location (km)
Oldman River near Brocket	WSC05AA024	6.2
Oldman River near Lethbridge	WSC05AD007	172.7
Saskatchewan River near Medicine Hat	WSC05AJ001	424.5

The WSC gauge record for the Oldman River near Brocket does not contain data for this event, likely due to gauge failure, given its proximity to the dam. However, the dam's operational record was provided by Alberta Environment (AENV), and this data provided sufficient information to define the upstream inflow boundary condition for the hydraulic model. Discharge data from the other gauges further downstream were used to evaluate the performance of the model. Figure 4.6a presents the discharge hydrographs at the latter two sites, along with the Oldman Dam outflow record, for the 1995 event. Tables of the data are provided in Appendix B (6 h intervals, as provided by AENV).

Water level records for these gauges would also be very useful for model validation. Unfortunately, no water level data was provided and such data is not published for these records on the WSC public site. Therefore, such comparisons could not be conducted. However, high water marks were obtained during the flood, providing at least some means of evaluating the model results in this regard.

As Figure 4.6a illustrates, substantial lateral inflows must have occurred between the Oldman Dam and Lethbridge and (to a lesser extent) between Lethbridge and Medicine Hat, given the obvious differences in direct runoff volume between the three hydrographs.

As seen in Figures 4.1, there are a number of tributaries within the study reach. There was no data available for the 1995 event for two of these tributaries: Willow Creek and the Little Bow River. However three of the tributaries are gauged: the St. Mary River and Belly Rivers upstream of Lethbridge, and the Bow River downstream of Lethbridge, as summarized in Table 4.4. Unfortunately, the gauge on the Belly River nearest the confluence (05AD002) was not operational during the event. Lateral inflows on the Belly River were therefore estimated by combining the gauge data near Glenwood (Belly River: WSC05AD041 and Waterton River: 05AD028). However, this approximation does not consider inflows below the gauges. Figure 4.6b presents the discharge hydrographs for those gauges that remained operational. The axes are the same as for Figure 4.6a, to facilitate comparison. Tables of the data are provided in Appendix B (6 h intervals, as provided by AENV).

As Figure 4.6b illustrates, the lateral inflows were relatively small compared to the overall event magnitude with the exception of, perhaps, the Bow River. However, in comparing them to the outflows from the Oldman Dam, it is clear that comparatively similar amounts of water entered the river downstream of the Dam as was released by the Dam during this event.

Table 4.3 Water Survey of Canada gauges on the tributaries

Tributary	Gauge name	Number	Longitude	Latitude
Belly	Waterton River near Glenwood	05AD028	113°28'10"	49°26'35"
Belly	Belly River near Glenwood	05AD041	113°28'49"	49°21'08"
St. Mary	St.Mary River near Lethbridge	05AE006	112°50'38"	49°34'24"
Bow	Bow River below Bassano Dam	05BM004	112°32'20"	50°45'00"

4.3 Numerical Model Setup

A *RIVER1D* input data file describing the channel geometry and resistance characteristics was prepared, using the data described above. Natural channel sections were input to the *RIVER1D* model in terms of top width versus elevation, as this is the format required by the model at present.

Hydraulic flood routing essentially amounts to unsteady flow modeling and in order to conduct such a simulation, one must specify the initial conditions occurring at the commencement of the simulation as well as specifying adequate flow information at the boundaries for the whole duration of the simulation. These aspects of the models are described below.

4.3.1 Boundary conditions

Two boundary conditions must be specified in any unsteady flow simulation of this type. Assuming that the flow is subcritical (as in this case) then this would typically require the input of an inflow hydrograph at the upstream boundary, and a stage hydrograph at the downstream boundary. Other inputs may be employed, but this requires significant knowledge of unsteady flow hydraulics, and as this would not be done in the typical flood routing application, it was not undertaken here.

As discussed earlier, the inflow hydrograph at the upstream boundary was determined based on the operational record at the Oldman Dam, since the nearest WSC gauge

(Oldman River at Brockett) did not provide a record for this event. A comparison for the data from both sources, for the period where there is overlap (just before and just after the event) indicates they are virtually identical.

The need for a water level hydrograph at the downstream end of the modeled reach presents an inconvenience, since one typically does not know what water levels will occur when using the models in a forecasting mode. To avoid the necessity for dealing with this, an artificial length of river was added at the downstream end of the modeled reach, by repeating the last cross section for an additional 200 km (again on 1 km intervals) and employing the same gradient as in the lowermost segment of the South Saskatchewan River. The water level at the new (fictitious) downstream boundary was then just set to an arbitrary subcritical flow depth. Essentially this new downstream boundary was set sufficiently far downstream of the modeled reach, so that it did not matter that the specified boundary condition there was inaccurate.

As discussed earlier, lateral inflow data was available for the Bow and St. Mary Rivers and inflows from the Belly River were estimated by combining the gauge data near Glenwood (Belly River: WSC05AD041 and Waterton River: 05AD028). No inflow data for Willow Creek or the Little Bow River was available for this particular event, but it would be an easy matter to include this type of data in future application of the models.

Often gauge sites for tributaries are located some distance upstream of the confluence, typically so as to be above the effects of backwater from the main river, although other reasons do sometimes apply as well (such as in this case where the lower gauge failed). In such cases, it is sometimes necessary to adjust flow magnitudes to account for

additional tributary drainage area downstream of the gauge site, and/or to lag the hydrograph to account for travel time from the actual gauge site to the confluence. Estimation of additional inflows downstream of tributary gauge sites was beyond the scope of this investigation; however, hydrograph lagging was investigated.

4.3.2 Initial conditions

Any unsteady flow simulation requires as input details of the initial conditions (stage and discharge) at every computational node. Initial discharges are easily obtained since they are simply the inflow rates (base flows) prior to the flood event. However, the corresponding water levels are not typically known at each computational node.

For the *RIVER1D* model, rather than conducting a separate steady flow water level profile analysis to determine these values, one can simply input estimates of the starting water levels and then run *RIVER1D* using the time stepping unsteady flow simulation to achieve the same objective. In this case a constant inflow discharge is specified along with a guess of the initial water levels, and the model is run until a steady water level profile is achieved. The results at intermediate time steps are not physically meaningful and thus not of interest, just the final steady state solution is needed to establish the initial conditions for the subsequent unsteady flow simulation. Consequently a lower convergence tolerance and/or fewer iterations per time step can be employed to help to speed up this preliminary model run. *RIVER1D* has been set up to do this automatically for the user.

4.3.3 Spatial and Temporal Discretization

As this was the first practical test of the new natural channel equation formulation in *RIVER1D*, a base case was established with the objective of obtaining a stable and accurate solution. As discussed earlier, unlike the earlier *cdg1-D* model (which employed a rectangular channel formulation) the natural channel formulation employs the proposed approximate conservation formulation. The magnitude of the error introduced by the approximation depends on the water surface slope and the specific channel geometry. The preceding error analysis provides a means of approximating this error and thus provides guidance for estimating appropriate section spacing. However, in general it is simplest to determine the appropriate spacing by a trial and error approach. In the Oldman River application it was found that, to ensure model stability and accuracy, sections spacing increments ranging from 100 to 500 m were necessary. That is, the approximate formulation required a reduction in discretization.

As equation (2.35) implies, decreasing section spacing generally requires a corresponding decrease in the time step increment to maintain an appropriate Courant number. However, as discussed earlier, this applies to the dynamic case and for diffusive waves (such as rainfall runoff events propagating over large distances) this stringent requirement can usually be greatly relaxed. However, in applying this new natural formulation version of *RIVER1D* to the Oldman River, it was found that time steps in excess of 5s would result in model failure (i.e. the solution would become unstable and "blow up"). This corresponds to a Courant number of only about 0.1. This illustrates a clear limitation of the *RIVER1D* model, since such a small time step is highly inefficient

(i.e. these simulations each took about 30h to run). The issue appears to be that the upwinding component of the model, which is designed to damp high frequency oscillations, is based on the dynamic terms in the equation only. Past research found that for simple geometry, the model was also stable for diffusive (friction dominated events). It appears that for the natural channel case, the upwinding component will need some redesign to incorporate friction effects into the upwinding.

4.4 Results in RIVER1D

4.4.1 General notes on model implementation

The CDG finite element scheme employed in this model selectively dampens high frequency, numerically generated, oscillations without damping actual physical wave components when a semi-implicit time discretization is used (Hicks ands Steffler, 1990). This corresponds to a θ of 0.5, which was used in all unsteady simulations conducted for the Oldman River. The upwinding parameter, ω, was set to 0.25 for this type of application, as that is what was recommended by Hicks and Steffler (1990). Although they observed that the damping was more selective for ω = 0.25 than for ω=0.5, in general they found that the impact of varying this parameter was marginal (Hicks and Steffler, 1992).

Summarizing, the base case scenario for the *RIVER1D* model simulations involved the following characteristics:

- time step increment, Δt = 5s

- spatial discretization, Δx = 100 to 500 m
- upwinding coefficient, ω = 0.25
- implicitness, θ = 0.5 (second order accurate)
- natural geometry used in the reach downstream of Oldman Dam, as well as at Lethbridge and at Medicine Hat
- rectangular channel geometry approximation used elsewhere
- tributary inflows based on data from gauges listed in Table 4.3, no lagging of hydrographs

It is significant to note that initial tests runs of the *RIVER1D* model, incorporating natural channel geometry for the Fort Mcleod reach, stable solutions could not be achieved. As discussed earlier, an investigation of the nature of the cross sections here raised some questions as to whether they are physically reasonable. In the end, the only way to actually successfully run the full model was to revert to the rectangular channel approximation at Fort Mcleod.

4.4.2 Model results

Figure 4.7 shows the output discharge hydrographs obtained from the *RIVER1D* model at Lethbridge and Medicine Hat for the base case scenario. The measured data is also shown for comparison. As the figure illustrates, for the peak flow, the arrival time of peak flow at both of the locations predicted by RIVER1D is early than the observed, and the magnitude of peak flow is less than the measured flow rate. Table 4.4 presents the quantitative errors on the peak magnitudes and arrival times calculated using:

$$error = \frac{Predicted\ value - Measured\ value}{Measured\ value} \tag{4.1}$$

Table 4.4 *RIVER1D* peak discharge errors for the base case simulation (1995 event)

Location	Arrival time of peak flow		Peak flow (m^3/s)		Error on Peak	
	Measured	*RIVER1D*	Measured	*RIVER1D*	Magnitude (%)	Timing (h)
Lethbridge	June-8 6:00	June-7 18:00	4836	3849	-12.2	-12
Medicine Hat	June-9 18:00	June-8 23:00	5345	4358	-18.5	-19

It is likely that the significant differences in timing and magnitude of peak flows is caused, at least in part, by the fact that the tributary inflow data is not only incomplete but it has also not been corrected to consider time of travel from the individual gauges to the tributary confluences. To explore this possibility, in order to have the clearest possible picture of the quality of the model's capabilities, additional simulations were conducted considering only the reach from Lethbridge to Medicine Hat. This reach contains only one significant tributary, the Bow River, for which gauge data was available below the Bassano Dam (located approximately 100 km upstream of the confluence with the Oldman River). This short reach simulation employed the actual gauge flow record at Lethbridge as the upstream boundary condition. Two runs were conducted: the first with no lagging of the Bow River inflow hydrograph, and the second involving lagging the Bow River hydrograph by 22h (determined as an average time of travel based on an analysis of gauge records for previous large floods). Figure 4.8 illustrates that the model performance is significantly improved in this case, supporting the assertion that a primary

source of error for the full reach simulation was inadequate quantification of tributary inflows.

Table 4.5 presents a quantitative comparison of peak magnitudes and timing, where it is seen that results are improved for the case where tributary hydrograph lagging was employed. However, overall, it appears that lagging the lateral inflow hydrograph for the Bow River had a minimal impact on the resulting hydrograph at Medicine Hat. This is likely because the inflow component for the Bow River was small compared to the flows on the Oldman River (as seen when comparing Figures 4.6 (a) and (b)). However, although the peak magnitude did not improve, the forecast timing of the peak was considerably better when the tributary hydrograph was lagged. These two factors suggest that substantially improved forecasts could be expected if comparable routing models were set up for the tributaries as well.

Table 4.5 *RIVER1D* peak discharge errors for the short reach simulation of 1995 event (with and without lagging of the Bow River)

Bow River	Arrival time of peak flow		Peak flow (m^3/s)		Error on Peak	
	Measured	*RIVER1D*	Measured	*RIVER1D*	Magnitude (%)	Timing (h)
no lagging	June-9 18:00	June-9 7:00	5345	5285	-1.1	-11
lag 22h	June-9 18:00	June-9 13:00	5345	5141	-3.8	-5

A key motivation for using natural channel geometry in sub-reaches is to enable the accurate determination of water levels for flood forecasting purposes. Unfortunately, water level hydrographs were not available at the Lethbridge and Medicine Hat gauges

(as discussed earlier) to assess the quality of model results in this regard. However, high water mark profiles were measured during the 1995 event and thus provide a means for comparison to the peak water level profiles. Figure 4.9 presents this comparison, where it is seen that the model does reasonably well for the short reach simulation (i.e. when lateral inflows are reasonably defined).

4.4.3 Model sensitivity

Manning's *n* is the only calibration parameter for the hydraulic model and therefore, it was desirable to explore the model's sensitivity to this parameter. As stated earlier, an initial value of 0.030 was estimated for this parameter throughout all of the routing reaches, and for the sub-reaches where surveyed channel geometry was available from floodplain studies (Lethbridge and Medicine Hat) channel roughness was based on the data from the calibrated floodplain study. Figure 4.10 and Table 4.6 illustrate the sensitivity of model results for a variety of resistance values, and suggests that the effects of varying resistance are minimal. These results, in combination with those shown in Figures 4.7 and 4.8, suggest that the model could be used in a predictive sense with the current values for Manning *n*, provided tributary inflows could be approximated reasonably well.

Table 4.6 Sensitivity of RIVER1D peak discharges to Manning's *n*

Location	Case	Arrival time of peak flow	Peak flow (m^3/s)		Error on Peak	
		RIVER1D	Measured	*RIVER1D*	Magnitude (%)	Timing (h)
Lethbridge	n - 0.005	June-7 17:00	4836	3905	-11.0	-13
	Base	June-7 18:00		3849	-12.2	-12
	n + 0.005	June-7 20:00		3774	-14.0	-10
	n + 0.01	June-7 21:00		3694	-15.8	-9
Medicine Hat	n - 0.005	June-8 19:00	5345	4375	-18.2	-23
	Base	June-8 23:00		4358	-18.5	-19
	n + 0.005	June-9 2:00		4303	-19.5	-16
	n + 0.01	June-9 4:00		4228	-20.9	-14

The only other parameter to be varied in the *RIVER1D* model is ω, the upwind weighting factor. A sensitivity analysis was also conducted on this parameter for the range of possible values (0.25 to 0.50), Table 4.7 and Figure 4.11 show the that the model results were visually indistinguishable over this range. Therefore, the default value of 0.25 can be used with confidence.

Table 4.7 Sensitivity of *RIVER1D* peak discharges to upwinding coefficient ω

Location	Case	Arrival time of peak flow	Peak flow (m^3/s)		Error on Peak	
	ω	*RIVER1D*	Measured	*RIVER1D*	Magnitude (%)	Timing (h)
Lethbridge	0.25	June-7 18:00	4836	3849	-12.2	-12
	0.50	June-7 18:00		3837	-12.5	-12
Medicine Hat	0.25	June-8 23:00	5345	4358	-18.5	-19
	0.50	June-8 23:00		4361	-18.4	-19

4.4.4 Discussion of results

Clearly the *RIVER1D* model provides reasonably accurate discharge and water level forecasts, provided the lateral (tributary) inflow hydrographs can be determined to a reasonable level of accuracy. The results here suggest that there may be some merit in employing hydraulic routing on the tributaries to facilitate this.

The model did not display any significant sensitivity to the one calibration parameter (Manning's n) nor to the only variable numerical parameter ω (the upwinding coefficient).

Although the results for the *RIVER1D* modeling effort were promising in terms of accuracy, it required a tiny time step increment (Δt =5s) to ensure solution stability. This results in a simulation period of approximately 30h on a typical PC, which is generally impractical. Small time steps are a necessary aspect of dynamic flow routing, but should not be necessary for modeling diffusive waves. It is believed that this problem is related to the upwinding matrix of the CDG finite element scheme, which currently is based on dynamic terms only, whereas this application is diffusive (friction dominated). Further research is recommended to explore this issue.

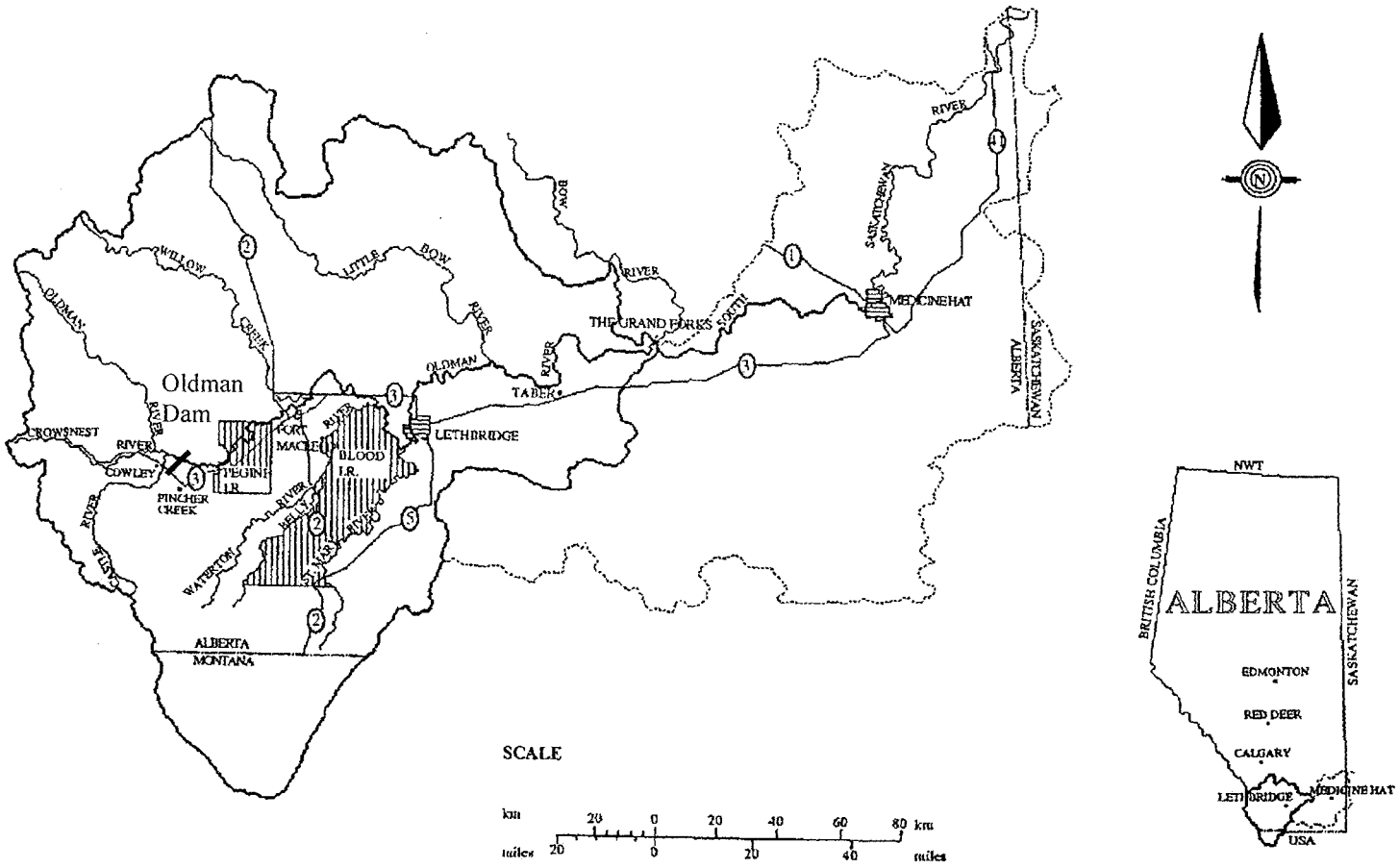

Figure 4.1 The Oldman and South Saskatchewan River Basin (adapted from McKay *et al.*, 1996).

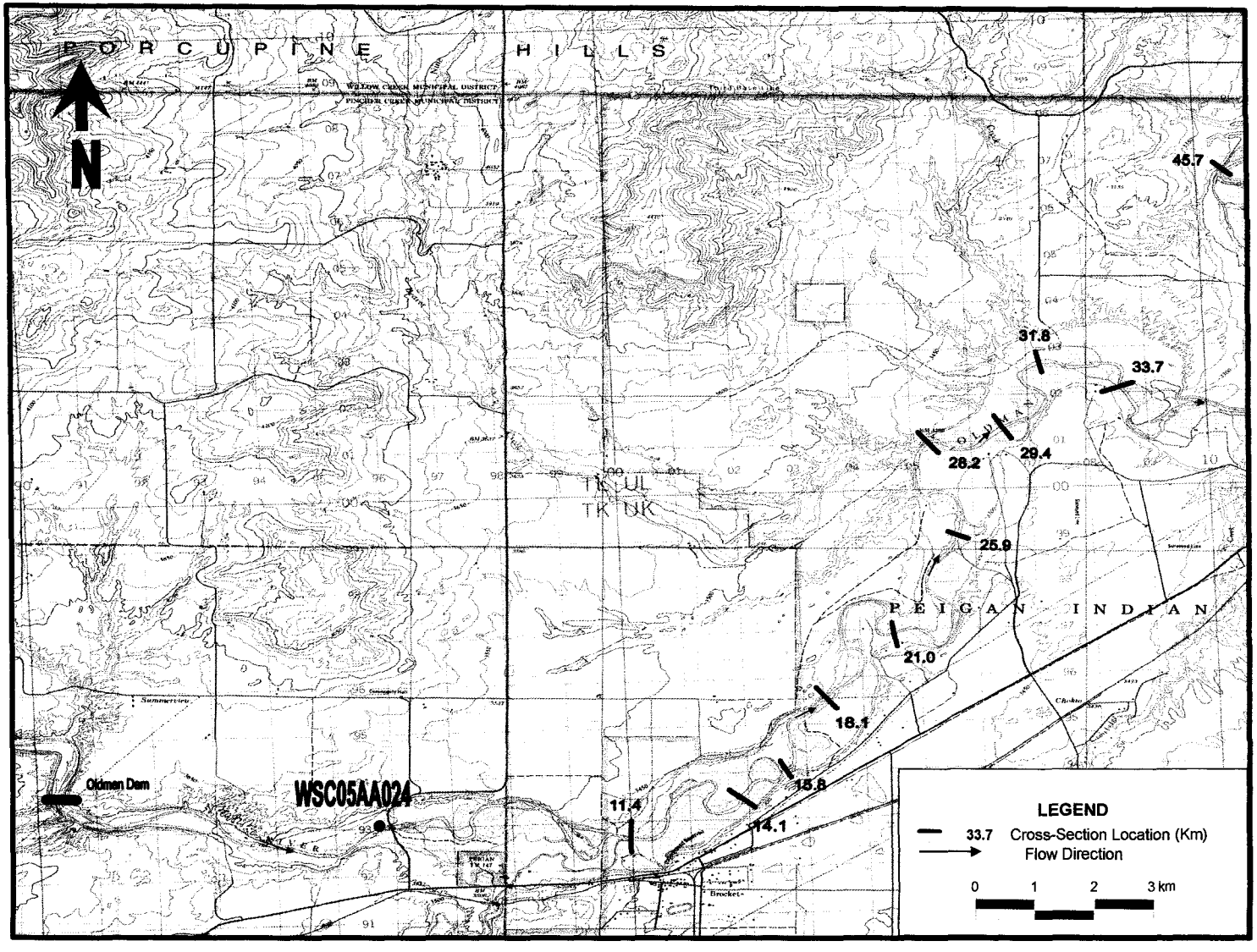

Figure 4.2 (a) Location map for cross sections in the vicinity of the Oldman Dam (upper portion).

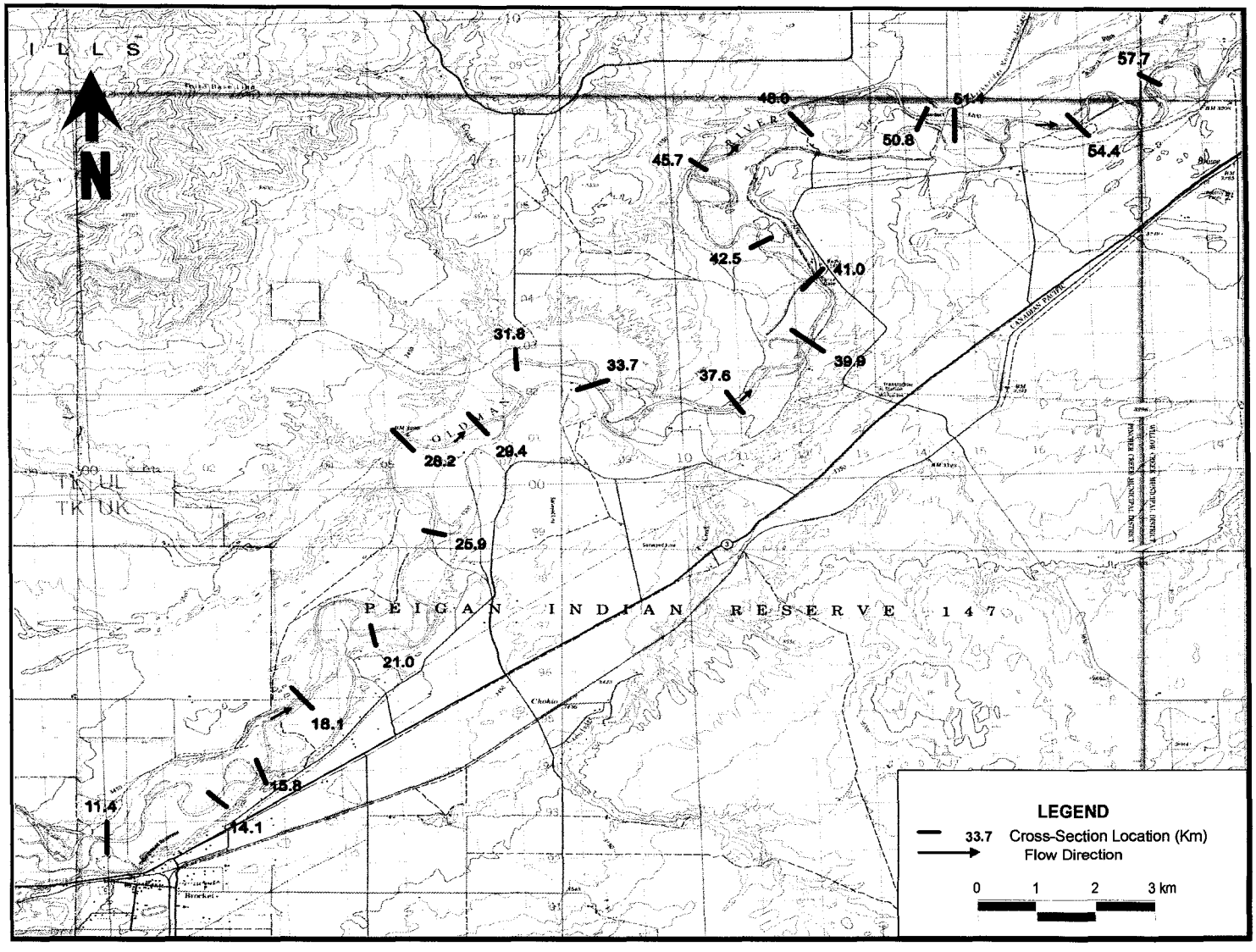

Figure 4.2 (b) Location map for cross sections in the vicinity of the Oldman Dam (lower portion).

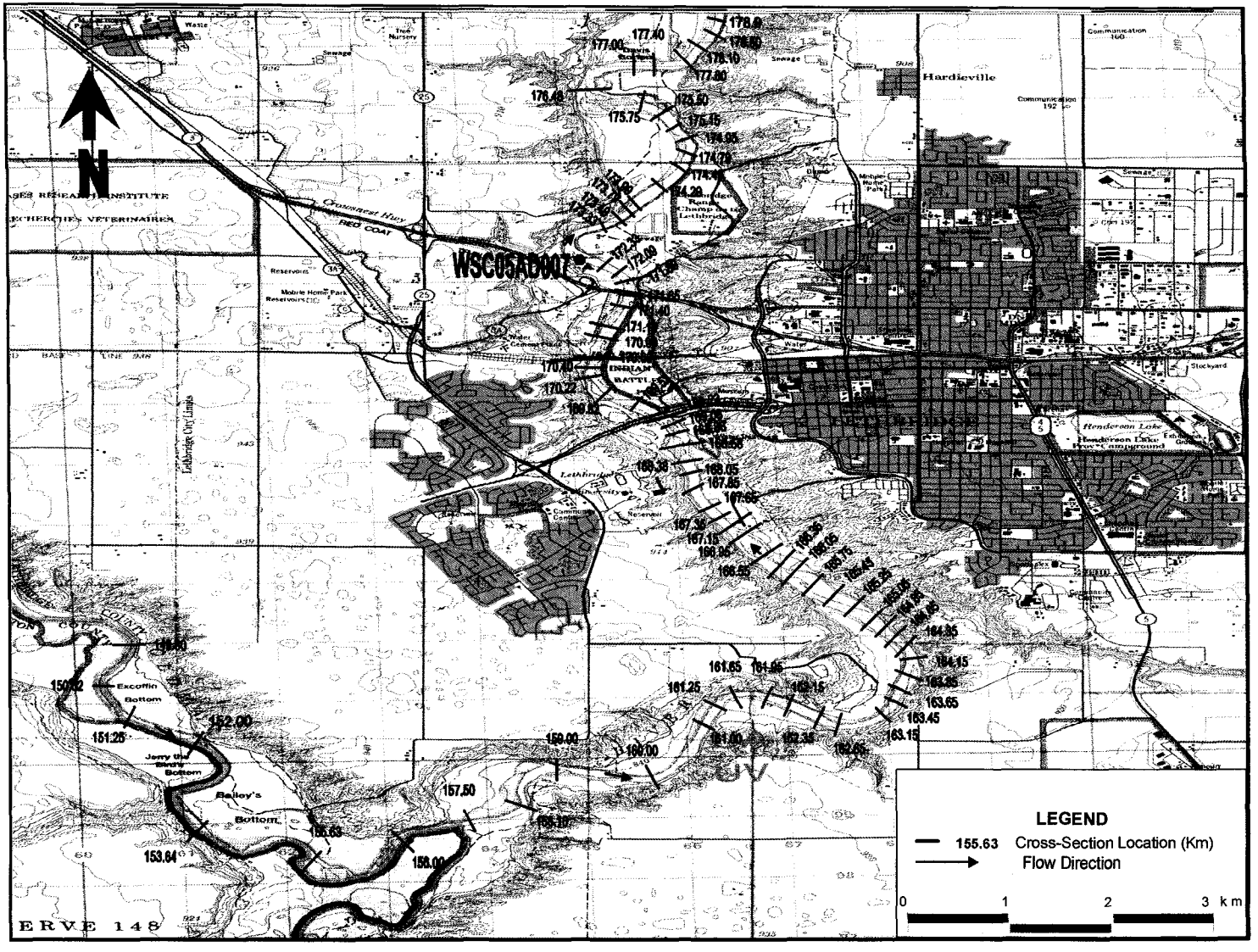

Figure 4.3 Location map for cross sections in the vicinity of Lethbridge.

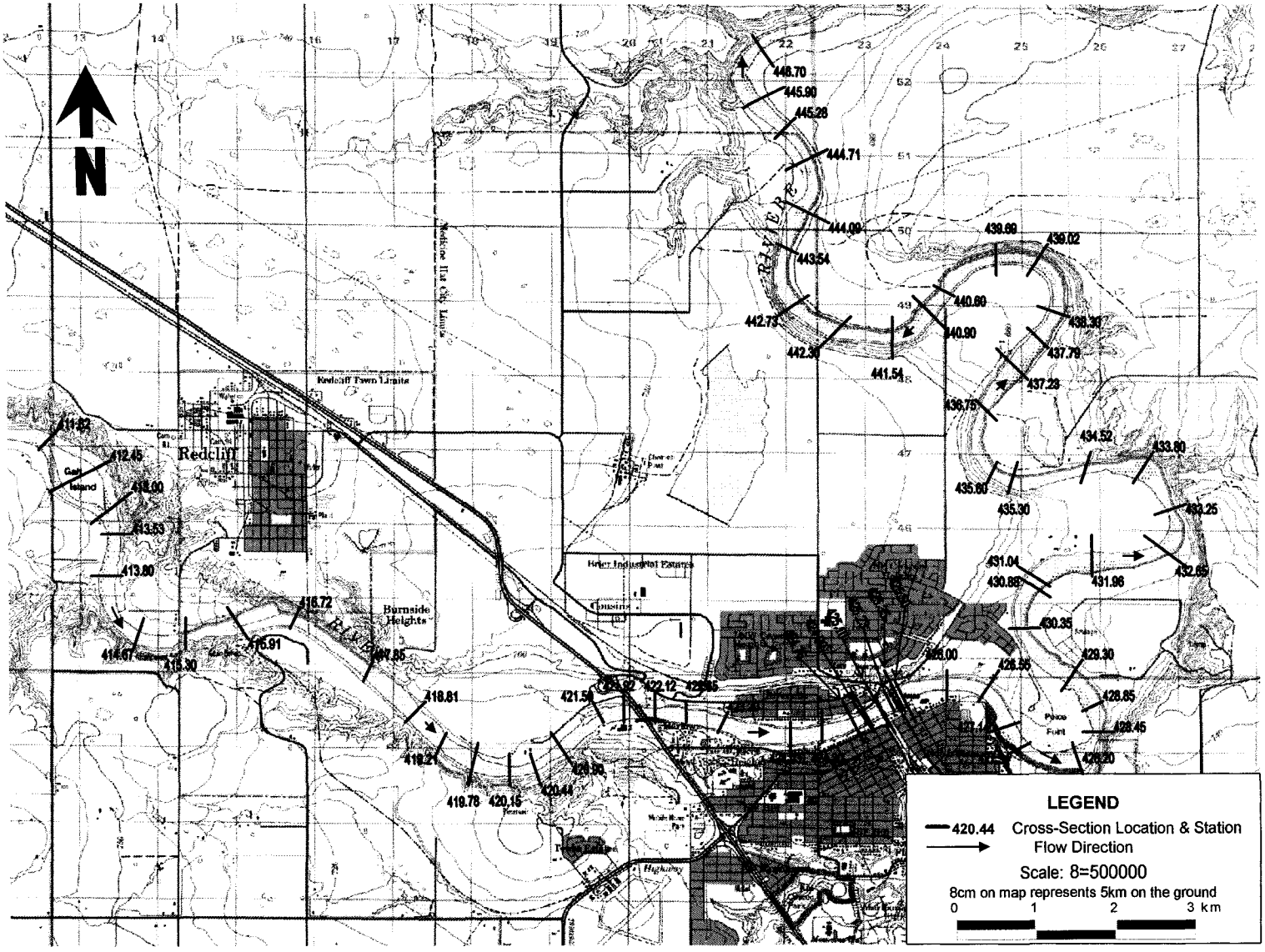

Figure 4.4 Location map for cross sections in the vicinity of Medicine Hat.

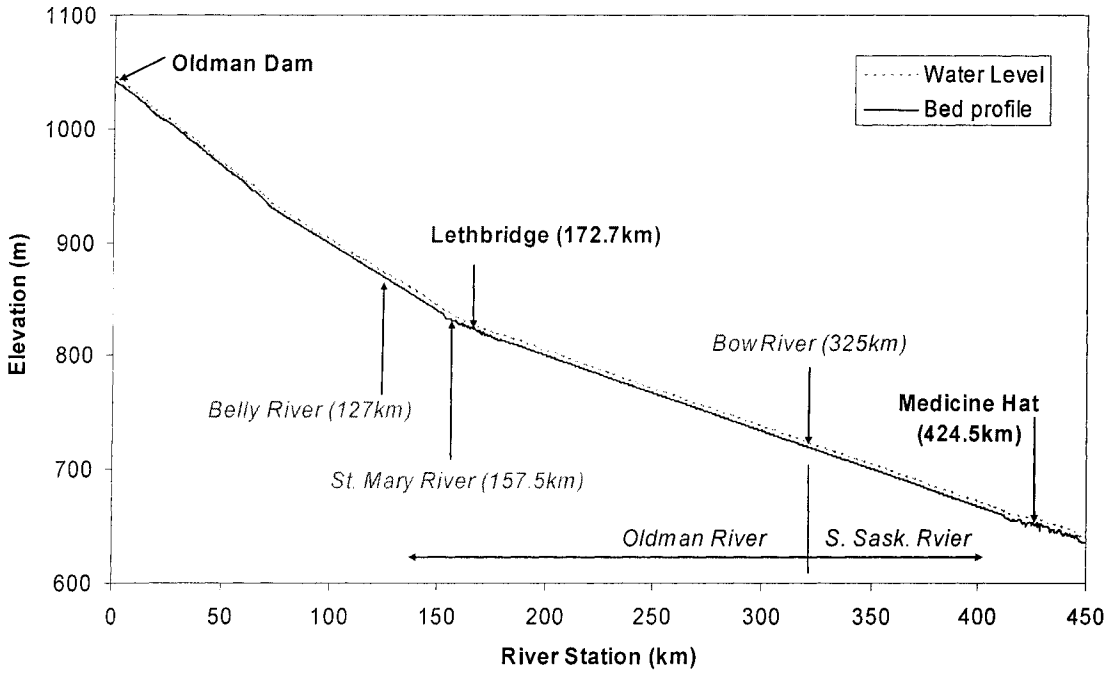

Figure 4.5 Bed Profile of the Oldman/South Saskatchewan River used in the *RIVER1D* model.

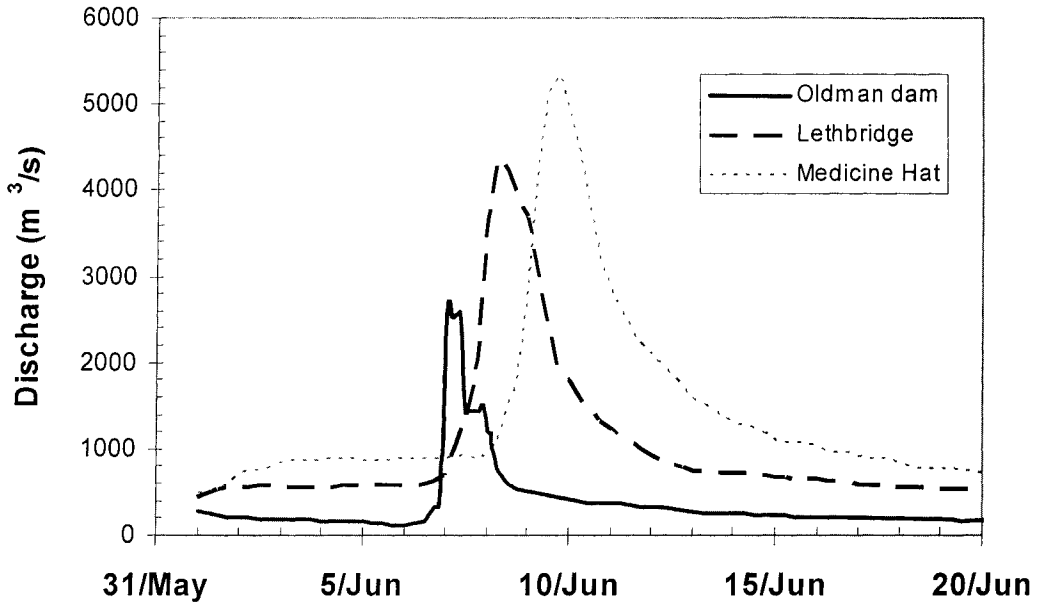

(a) Flows on the Oldman and South Saskatchewan Rivers.

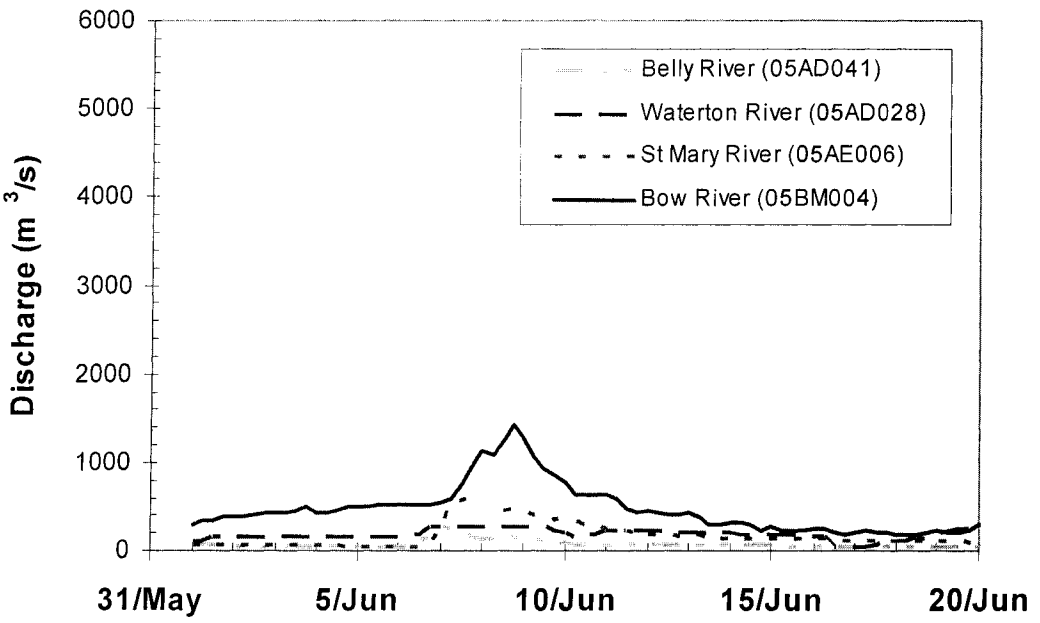

(b) Lateral inflows to the Oldman and South Saskatchewan Rivers.

Figure 4.6 Flows measured during the 1995 flood in the Oldman and South Saskatchewan River basins.

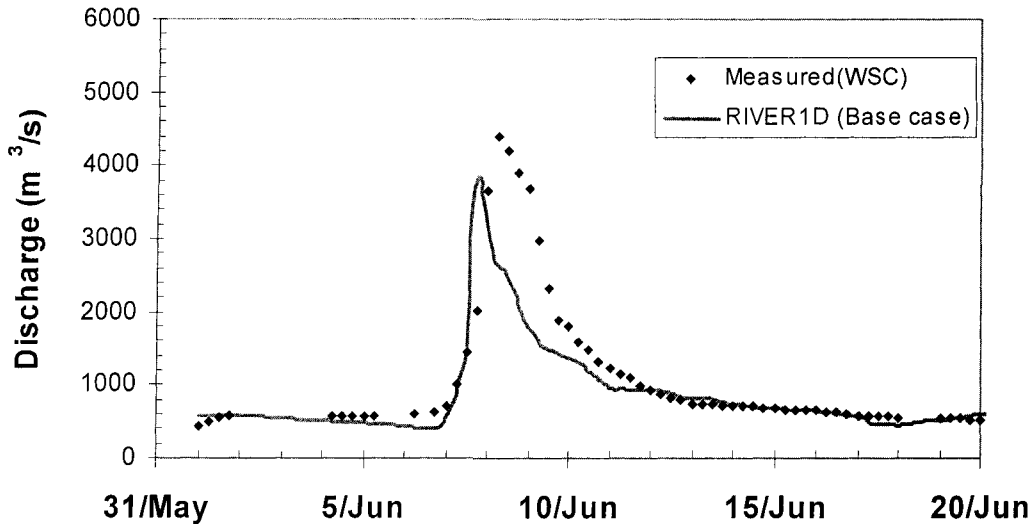

(a) Lethbridge

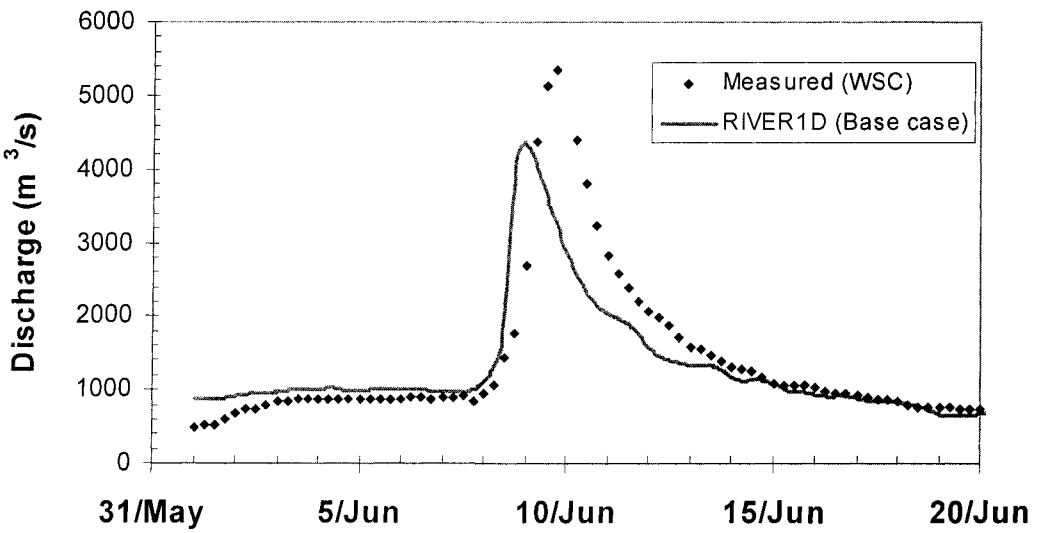

(b) Medicine Hat

Figure 4.7 Comparison of *RIVER1D* results to measured discharge hydrographs. (base case: Δt=5s, θ=0.5, ω=0.25, upstream boundary at Oldman Dam).

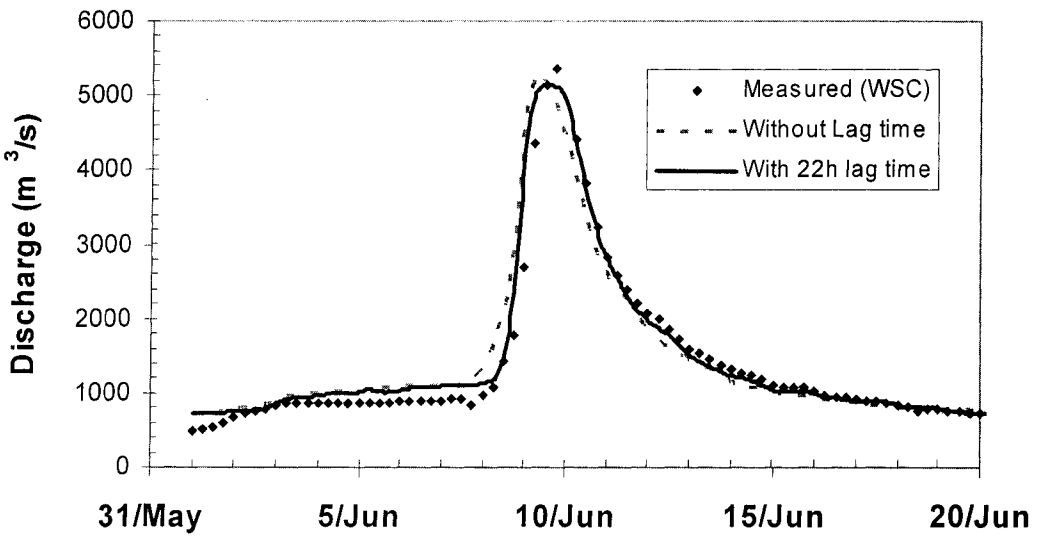

Figure 4.8 Comparison of *RIVER1D* results to measured discharge hydrograph at Medicine Hat (Δt=5s, θ=0.5, ω=0.25, upstream boundary at Lethbridge).

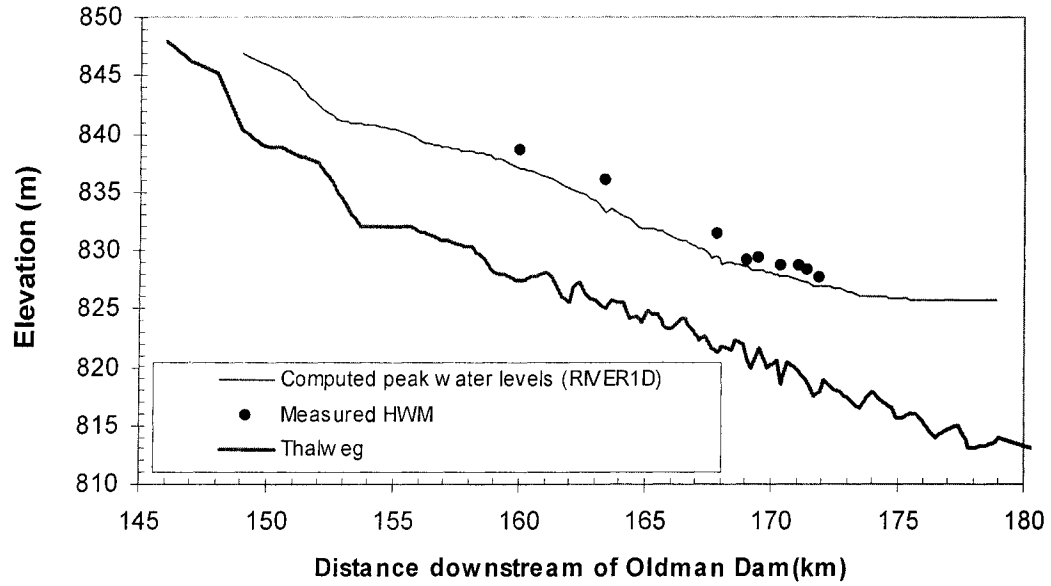

(a) Lethbridge

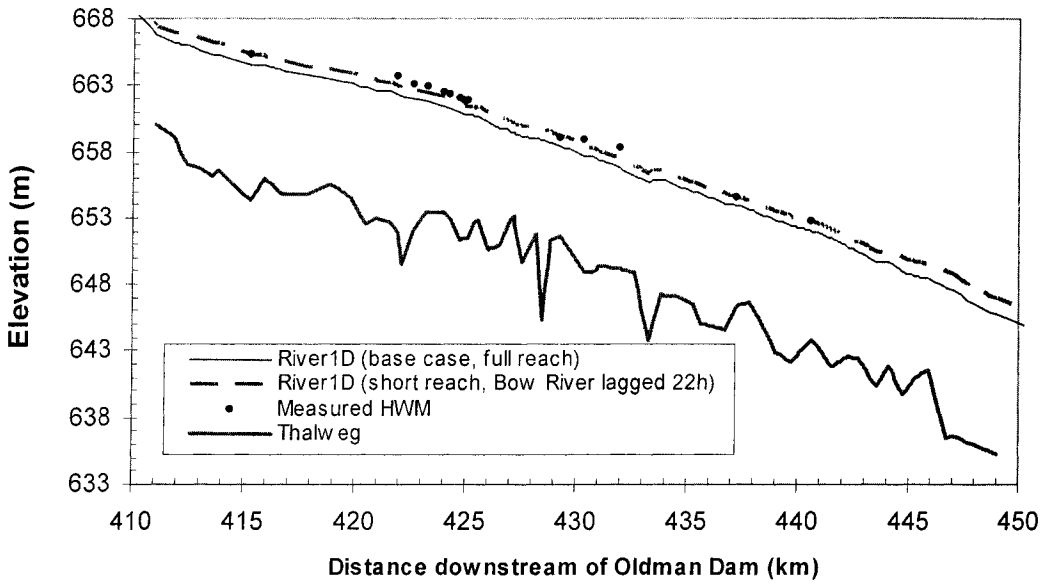

(b))Medicine Hat

Figure 4.9 Comparison peak water level results from *RIVER1D* to measured high water marks profiles at Lethbridge and Medicine Hat (Δt=5s, θ=0.5, ω=0.25).

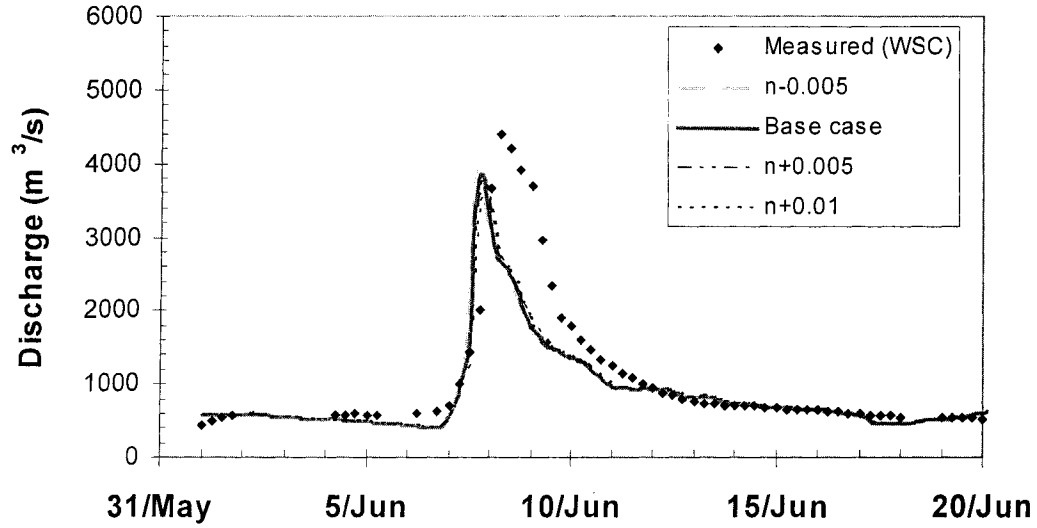

(a) Lethbridge

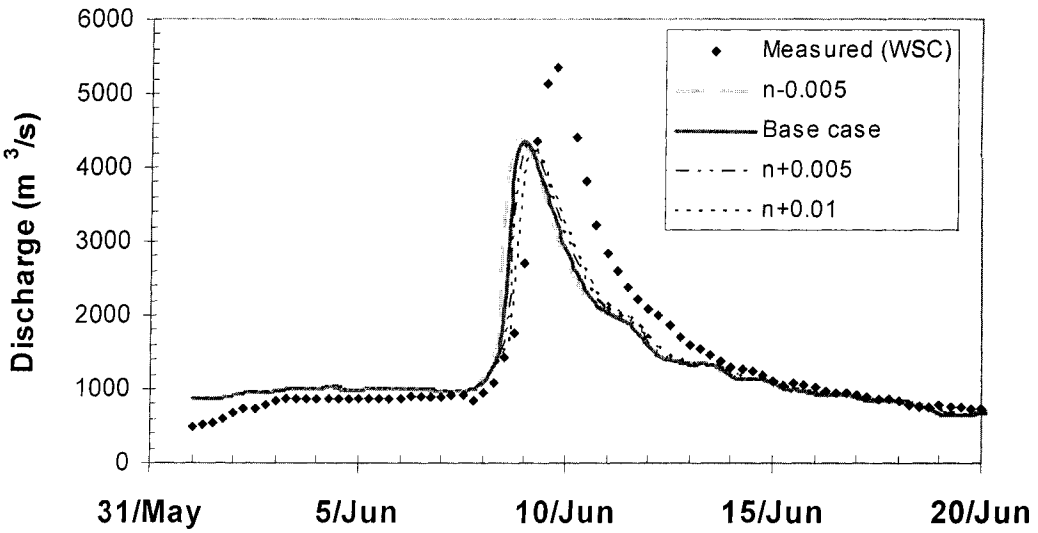

(b) Medicine Hat

Figure 4.10 Sensitivity of *RIVER1D* discharge results for varying channel resistance (Δt=5s, θ=0.5, ω=0.25, upstream boundary at Oldman Dam).

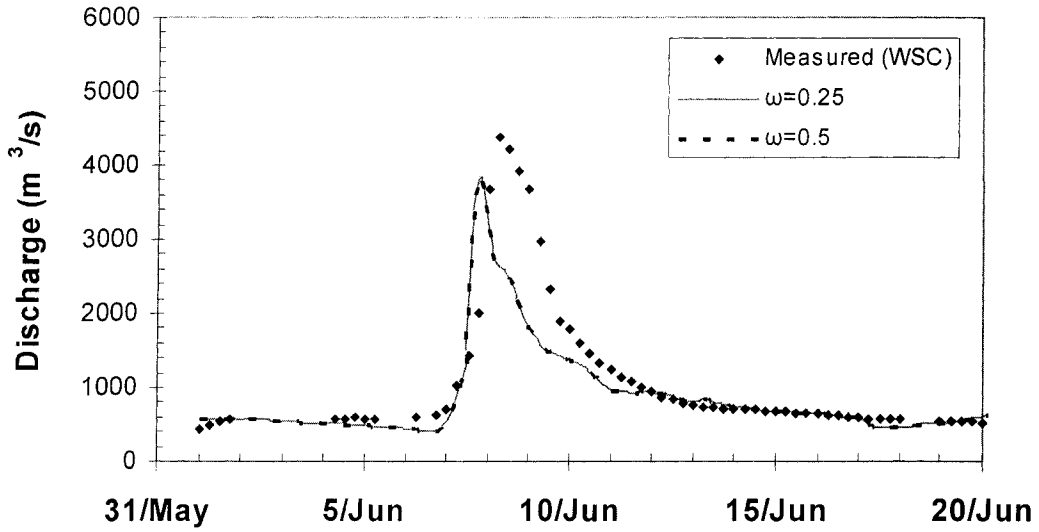

(a) Lethbridge

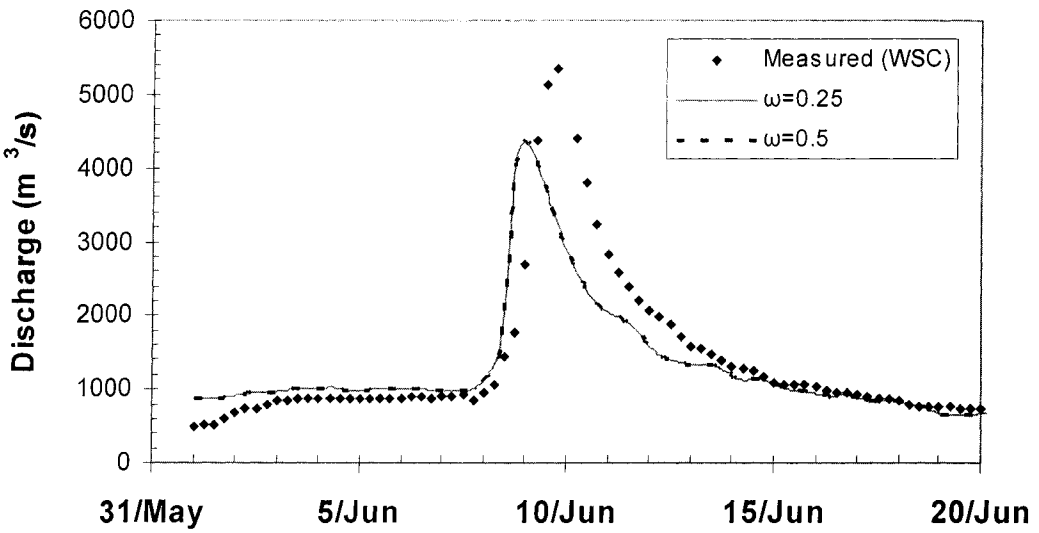

(b) Medicine Hat

Figure 4.11 *RIVER1D* discharge results for varying upwinding weighting factor (Δt=5s, θ=0.5, ω=0.25, upstream boundary at Oldman Dam).

CHAPTER 5

CONCLUSIONS AND RECOMMENDATIONS

5.1 Conclusions

This investigation considers a modified form of the St. Venant equation, in which effects of inclination and nonprismaticity are incorporated into an approximate term to ensure implementation of the conservative formulation. The source terms accounting for the width variation and bed slope are transferred to a flux term, which has the numerical advantage of facilitating the implementation of a finite element solution, circumventing the difficulty in treatment of lateral and bottom pressure for arbitrary geometry.

An error analysis provides a means of quantifying the error associated with the approximate formulation for variable width rectangular channels. The magnitude of the error depends on the water surface slope and the specific channel geometry, and, based on typical examples, it is clear that the error will be relatively small for most situations, suggesting that the proposed approximate formulation would be reasonably accurate ever for hydraulic jumps and steep surge waves. For general non-prismatic channel geometries, an approximate error evaluation can be made by exploiting the third order convergence of the pressure approximation. The approximate error can then be used as a criterion for refinement of the discretization in practical applications.

Energy loss evaluation for the approximate formulation was accomplished for the case sudden expansions and contractions in rectangular channels. Instead of using the average water surface elevation, a more general formula is proposed to calculate the constant water surface elevation when evaluating the pressure acting on the wetted boundary surface. The results indicate that α=1 is more accurate than α=0.5 in this case. As the variation of cross section includes gradual and sudden transition in real rivers, the weighting coefficient α for natural channel is recommended in a range of $0.5 \leq \alpha \leq 1$.

The shock capturing capability of the approximate formulation was demonstrated for both steady and unsteady flow situations. The implementation was illustrated using the finite element method, for which this approximate equation formulation adapts naturally. Using the Characteristic-Dissipative-Galerkin scheme, good results were obtained for the case of a hydraulic jump in a diverging rectangular channel, with the maximum percent error associated with the approximate formulation determined to be only 0.34%. For the case of dam break wave propagation in a converging and diverging rectangular channel, the model performed similarly well, with the maximum error only 0.0064%. In addition, the simulations involving the flow transition (from a mild to a steep sloped channel) and for a classic dam break in a prismatic channel, further demonstrated the validity of the proposed approximate formulation and finite element implementation.

The primary objective in developing this approximate formulation was to facilitate flow simulation in arbitrary geometry natural channels. To evaluate its potential, the proposed formulation was applied to a real river-flood routing problem, specifically the

Oldman/South Saskatchewan River in Southern Alberta. For the full reach, due to the inaccurate tributary inflow data, the predicted peak magnitudes are lower than the observed, and arrive earlier. To more accurately illustrate the model's capabilities, a shorter reach was simulated as well, one for which tributary inflows could be more accurately defined, and this was found to improved model agreement with measured data. Additional testing, involving lagging of the tributary hydrograph to account for time of travel from the tributary's gauge site to its confluence with the main river, illustrated the importance of accurate tributary data in routing applications of this type. The model itself appears to perform extremely well, and shows no great sensitivity to the only calibration parameter (channel roughness) or to the numerical upwinding parameter (ω). Furthermore, it shows reasonable agreement with the high water marks measured during the flood (again, for the case where tributary flows could be reasonably accurately determined). Therefore, this model should be useable in a predictive sense.

5.2 Recommendations

The main outstanding limitation in the application of hydraulic flood routing is the issue of determining sufficiently accurate tributary inflows as tributary inflow is a key factor in determining accurate forecasts. As gauge failure is a common occurrence during extreme floods, consideration should be given to developing similar hydraulic models of the tributaries, so that flows could at least be routed down to the confluences.

In terms of the model itself, it appears that the primary outstanding limitation is in terms of computational efficiency. Although the model appears to produce accurate results, the time step constraint (particularly on the diffusive wave simulation for the Oldman River) is unrealistic. It is believed that this problem is related to the nature of the upwinding matrix of the CDG finite element scheme, which currently is based on dynamic terms only. Flood routing problems are friction dominated and there is no consideration of this in the current upwinding matrix. Further research is recommended to explore this issue.

REFERENCES

Bellos, C. V., Soulis, J. V., and Sakkas, J. G. (1992). "Experimental investigation of two-dimensional dam-break induced flows." *Journal of Hydraulic Research*, 30(1), 47-63.

Blackburn, J. L. (2000). "Forecasting open water and ice related flood events using hydraulic modeling techniques," Master of Science, University of Alberta, Edmonton, Alberta

Blackburn, J. L., and Hicks, F. E. (2002). "Combined flood routing and flood level forecasting." *Canadian Journal of Civil Engineering*, 29(1), 64-75.

Capart, H., Eldho, T. I., Huang, S. Y., Young, D. L., and Zech, Y. (2003). "Treatment of natural geometry in finite volume river flow computations." *Journal of Hydraulic Engineering*, 129(5), 385-393.

Cunge, J. A., Holly, F. M., and Verwey, A. (1980). *Practical aspects of computational river hydraulics*, Pitman Publishing Limited, London.

Fennema, R. J., and Chaudhry, M. H. (1987). "Simulation of one-dimensional Dam-Break flows." *Journal of Hydraulic Research*, 25(1), 41-51.

Fread, D. J. (1988). "The NWS DAMBRK model:Theoretical background/user documentation." Office of Hydrology, National Weather Service(NWS), Maryland.

Garcia-Navarro, P., and Vazquez-Cendon, M. E. (2000). "On numerical treatment of the source terms in the shallow water equations." *Comput. Fluids*, 29, 951-979.

Henderson, F. M. (1966). *Open Channel Flow*, Macmillan Publishing CO., INC, New York.

Hicks, F. E., and Steffler, P. M. (1990). "Finite element modeling of open channel flow." Water Resour. Engrg. Report No. 90-6, Dept. of Civil Engineering, University of Alberta, Edmonton, Alberta .

Hicks, F. E., and Steffler, P. M. (1992). "Characteristic dissipative Galerkin scheme for open-channel flow." *Journal of Hydraulic Engineering*, 118(2), 337-352.

Hicks, F. E., and Steffler, P. M. (1994). "Comparison of finite element methods for the St.Venant equations." *International Journal for Numerical Methods in Fluids*, 20(2), 99-113.

Hicks, F. E., and Steffler, P. M. (1995). "Comparison of finite element methods for the St.Venant equations." *International Journal for Numerical Methods in Fluids*, 20(2), 99-113.

Hicks, F. E., Chen, J., and Barbar, N. (2005). "Hydraulic Flow Routing, Oldman River" Report Prepared for Water Resources Users Group, Alberta Environment, Edmonton, AB, Canada.

Katopodes, N. D. (1984). "A dissipative Galerkin scheme for open-channel flow." *Journal of Hydraulic Engineering*, 110(4), 450-466.

Kellerhals, R., Neill, C. R., and Bray, D. I. (1972). "Hydraulic and geomorphic characteristics of rivers in Alberta." Research Council of Alberta, River Engineering and Surface Hydrology Report 72-1, Edmonton, Alberta.

Khalifa, A. M. (1980). "Theoretical and experimental study of the radial hydraulic jump," PhD thesis, University of Windsor, Windsor,Ont., Canada.

KHAN, A., AZIZ., and Steffler, P. M. (1995). "Modeling rapidly varied open channel flows," PhD thesis, University of Alberta, Edmonton, Alberta .

Liggett, J. A., and Cunge, J. A. (1975). "Numerical methods of solution of the unsteady flow equations." Unsteady Flow in Open Channels, K. Mahmood and V. Yevjevich, eds., Water Resources Publications, Fort Collins, Colorado, 89-182.

McKay, K., S. Mikolajczyk, and Hicks, F. E. (1996). "Application of hydraulic flood routing techniques to the 1995 flood in Southern Alberta." *Proceeding, CSCE Annual Conference, Edmonton, Alberta,132-142.*

Sanders, B. F. (2001). "High-resolution and non-oscillatory solution of the St. Venant equations in non-rectangular and non-prismatic channels." *Journal of Hydraulic Research*, 39(3), 321-331.

Sanders, B. F., Jaffe, D. A., and Chu, A. K. (2003). "Discretization of integral equations describing flow in nonprismatic channels with uneven beds." *Journal of Hydraulic Engineering*, 129(3), 235-244.

Tseng, M.-H., Hsu, C.-A., and Chu, C. R. (2001). "Channel routing in open-channel flows with surges." *Journal of Hydraulic Engineering*, 127(2), 115-122.

Ying, X., Khan, A. A., and Wang, S. S. Y. (2004). "Upwind conservative scheme for the Saint Venant equations." *Journal of Hydraulic Engineering*, 130(10), 977-987.

Younus, M., and Chaudhry, M. H. (1994). "A depth-averaged k-ε turbulence model for the computation of free-surface flow." *Journal of Hydraulic Research,* 32(3), 415-444.

U.S. Corps of Engineers 2002. HEC-RAS River Analysis System, Hydraulic reference manual. Hydraulic Engineering Center Report CPD-69, Davis California.

APPENDIX A

IMPLEMENTATION OF CDG FINITE ELEMENT METHOD

The given conservative St.Venant equations are

$$\frac{\partial A}{\partial t}+\frac{\partial Q}{\partial x}=0 \tag{2.1}$$

$$\frac{\partial Q}{\partial t}+\frac{\partial}{\partial x}\left(\frac{Q^2}{A}+g\left(I_1-I_{1\bar{H}}\right)\right)=-gAS_f \tag{2.27}$$

And non-conservative forms of momentum equation (2.27) is rewritten as follows

$$\frac{\partial Q}{\partial t}+2U\frac{\partial Q}{\partial x}-U^2\frac{\partial A}{\partial x}+\frac{\partial}{\partial x}\left(gI_1-gI_{1\bar{H}}\right)+gAS_f=0 \tag{A.1}$$

In the Petrov-Galerkin method, the test function is

$$v_i=f_i+g_i \tag{A.2}$$

in which,

$$g_i=\omega\mathbf{W}\frac{\Delta x}{2}\frac{df_i}{dx} \tag{A.3}$$

in which ω=upwinding coefficient, $\mathbf{W}$=upwinding matrix, Δx =space step.

The equivalent Bubnov-Galerkin formulation is

$$\begin{bmatrix} f_i & 0 \\ 0 & f_i \end{bmatrix} \begin{Bmatrix} C \\ M \end{Bmatrix} + \omega \frac{\Delta x}{2} [\mathbf{W}] \frac{d}{dx} \begin{bmatrix} f_i & 0 \\ 0 & f_i \end{bmatrix} \begin{Bmatrix} C \\ M \end{Bmatrix} = \{0\} \tag{A.4}$$

in which C and M represents the continuity and momentum equation, respectively.

$$[\mathbf{W}] = \begin{bmatrix} w_{aa} & w_{aq} \\ w_{qa} & w_{qq} \end{bmatrix} \tag{A.5}$$

Equation (A.4) can be expanded as:

For the continuity equation:

$$f_i C + \omega \frac{\Delta x}{2} w_{aa} \frac{df_i}{dx} C + \omega \frac{\Delta x}{2} w_{aq} \frac{df_i}{dx} M = 0 \tag{A.6}$$

For the momentum equation:

$$f_i M + \omega \frac{\Delta x}{2} w_{qa} \frac{df_i}{dx} C + \omega \frac{\Delta x}{2} w_{qq} \frac{df_i}{dx} M = 0 \tag{A.7}$$

Hence, the weak statement for equation (2.1) and (2.27) are

$$\int_L \left\{ \begin{array}{l} f_i\left(\frac{\partial A}{\partial t}+\frac{\partial Q}{\partial x}\right)+\omega\frac{\Delta x}{2}w_{aa}\frac{df_i}{dx}\left(\frac{\partial A}{\partial t}+\frac{\partial Q}{\partial x}\right) \\ +\omega\frac{\Delta x}{2}w_{aq}\frac{df_i}{dx}\left[\frac{\partial Q}{\partial t}+2U\frac{\partial Q}{\partial x}-U^2\frac{\partial A}{\partial x}+\frac{\partial}{\partial x}\left(gI_1-gI_{1\bar{H}}\right)+fQ\right] \end{array} \right\} dx = 0 \quad \text{(A.8)}$$

$$\int_L \left\{ \begin{array}{l} f_i\left[\frac{\partial Q}{\partial t}+\frac{\partial}{\partial x}\left(Q^2/A+gI_1-gI_{1\bar{H}}\right)+fQ\right]+\omega\frac{\Delta x}{2}w_{qa}\frac{df_i}{dx}\left(\frac{\partial A}{\partial t}+\frac{\partial Q}{\partial x}\right) \\ +\omega\frac{\Delta x}{2}w_{qq}\frac{df_i}{dx}\left[\frac{\partial Q}{\partial t}+2U\frac{\partial Q}{\partial x}-U^2\frac{\partial A}{\partial x}+\frac{\partial}{\partial x}\left(gI_1-gI_{1\bar{H}}\right)+fQ\right] \end{array} \right\} dx = 0 \quad \text{(A.9)}$$

in which

$$f=\frac{|U|}{C_*^2 R} \quad \text{(A.10)}$$

where R = hydraulic radius, C_*=non- dimensional Chezy coefficient.

Integration by part and substitution of interpolation function $Q=f_jQ_j$, $A=f_jA_j$ gives

$$\begin{array}{l} \sum_e^{N_e}\int_e\left[f_if_j\frac{\partial A_j}{\partial t}dx-f_jQ_j\frac{df_i}{dx}dx+\omega\frac{\Delta x}{2}w_{aa}\frac{df_i}{dx}\left(f_j\frac{\partial A_j}{\partial t}+Q_j\frac{df_j}{dx}\right)\right]dx \\ +\sum_e^{N_e}\int_e\omega\frac{\Delta x}{2}w_{aq}\frac{df_i}{dx}\left[\begin{array}{l} f_j\frac{\partial Q_j}{\partial t}+a_{qq}Q_j\frac{df_j}{dx}+a_{qa}A_j\frac{df_j}{dx} \\ +\frac{\partial}{\partial x}\left(gI_1-gI_1|_{\bar{H}}\right)+ff_jQ_j \end{array}\right]dx+\sum_e^{N_e}\left[f_if_jQ_j\right]_e=0 \end{array} \quad \text{(A.11)}$$

$$\sum_{e}^{N_e}\int_e f_i f_j \frac{\partial Q_j}{\partial t}dx+\sum_{e}^{N_e}\left[f_i f_j Q_j U\right]_e-\sum_{e}^{N_e}\int_e f_j Q_j U\frac{df_i}{\partial x}dx+\sum_{e}^{N_e}\left[f_i\left(gI_1-gI_{1\bar{H}}\right)\right]_e$$

$$+\sum_{e}^{N_e}\int_e\left[-\left(gI_1-gI_{1\bar{H}}\right)\frac{df_i}{\partial x}+ff_i f_j Q_j+\omega\frac{\Delta x}{2}w_{qa}\frac{df_i}{dx}\left(f_j\frac{\partial A_j}{\partial t}+Q_j\frac{df_j}{dx}\right)\right]dx \qquad \text{(A.12)}$$

$$+\sum_{e}^{N_e}\int_e\omega\frac{\Delta x}{2}w_{qq}\frac{df_i}{dx}\left[f_j\frac{\partial Q_j}{\partial t}+a_{qq}Q_j\frac{df_j}{dx}+a_{qa}A_j\frac{df_j}{dx}+\frac{\partial}{\partial x}\left(gI_1-gI_{1\bar{H}}\right)+ff_j Q_j\right]dx=0$$

in which

$$[\mathbf{A}]=\begin{bmatrix}a_{aa} & a_{aq}\\ a_{qa} & a_{qq}\end{bmatrix}=\begin{bmatrix}0 & 1\\ -U^2 & 2U\end{bmatrix} \qquad \text{(A.13)}$$

Rearrange of the equations above

$$\sum_{e}^{N_e}\int_e\left(f_i f_j+\omega\frac{\Delta x}{2}w_{aa}\frac{df_i}{dx}f_j\right)\frac{\partial A_j}{\partial t}dx+\sum_{e}^{N_e}\int_e\omega\frac{\Delta x}{2}w_{aq}\frac{df_i}{dx}f_j\frac{\partial Q_j}{\partial t}dx$$

$$+\sum_{e}^{N_e}\int_e\omega\frac{\Delta x}{2}w_{aq}\frac{df_i}{dx}\left(a_{qa}\frac{df_j}{dx}\right)A_j dx+\sum_{e}^{N_e}\int_e\omega\frac{\Delta x}{2}w_{aq}\frac{df_i}{dx}\left(\frac{\partial}{\partial x}\left(gI_1-gI_{1\bar{H}}\right)\right)dx$$

$$+\sum_{e}^{N_e}\int_e\left(-f_j\frac{df_i}{dx}+\omega\frac{\Delta x}{2}w_{aa}\frac{df_i}{dx}\frac{df_j}{dx}+\omega\frac{\Delta x}{2}w_{aq}\frac{df_i}{dx}\left(a_{qq}\frac{df_j}{dx}+ff_j\right)\right)Q_j dx+\sum_{e}^{N_e}\left[f_i f_j Q_j\right]_e=0$$

(A.14)

$$\sum_{e}^{N_e} \int_e \omega \frac{\Delta x}{2} w_{qa} \frac{df_i}{dx} f_j \frac{\partial A_j}{\partial t} dx + \sum_{e}^{N_e} \int_e \left(f_i f_j + \omega \frac{\Delta x}{2} w_{qq} \frac{df_i}{dx} f_j \right) \frac{\partial Q_j}{\partial t} dx$$

$$+ \sum_{e}^{N_e} \int_e \left(\omega \frac{\Delta x}{2} w_{qq} \frac{df_i}{dx} \left(a_{qa} \frac{df_j}{dx} \right) \right) A_j dx$$

$$+ \sum_{e}^{N_e} \int_e \left(-f_j U \frac{df_i}{dx} + ff_i f_j + \omega \frac{\Delta x}{2} w_{qa} \frac{df_i}{dx} \frac{df_j}{dx} + \omega \frac{\Delta x}{2} w_{qq} \frac{df_i}{dx} \left(a_{qq} \frac{df_j}{dx} + ff_j \right) \right) Q_j dx \quad \text{(A.15)}$$

$$+ \sum_{e}^{N_e} \left[f_i f_j Q_j U \right]_e + \sum_{e}^{N_e} \left[f_i \left(gI_1 - gI_{1\bar{H}} \right) \right]_e$$

$$+ \sum_{e}^{N_e} \int_e \omega \frac{\Delta x}{2} w_{qq} \frac{df_i}{dx} \left(\frac{\partial}{\partial x} \left(gI_1 - gI_1|_{\bar{H}} \right) \right) dx - \sum_{e}^{N_e} \int_e \left(gI_1 - gI_{1\bar{H}} \right) \frac{df_i}{\partial x} dx = 0$$

In matrix notation, equation (A.14) and (A.15) rewrite as

$$\mathbf{S} \frac{\partial \Phi_j}{\partial t} + \mathbf{K} \Phi_j + \mathbf{f} = 0 \quad \text{(A.16)}$$

The mass matrix $\mathbf{S} = \sum_{e=1}^{N_e} \mathbf{S}_e$ and $\mathbf{S}_e = \begin{bmatrix} S_{aa} & S_{aq} \\ S_{qa} & S_{qq} \end{bmatrix}$, in which

$$[S_{aa}]=\left[\int_e \left(f_i f_j+\omega\frac{\Delta x}{2}w_{aa}\frac{df_i}{dx}f_j\right)dx\right]$$

$$[S_{aq}]=\left[\int_e \omega\frac{\Delta x}{2}w_{aq}\frac{df_i}{dx}f_j dx\right]$$

$$[S_{qa}]=\left[\int_e \omega\frac{\Delta x}{2}w_{qa}\frac{df_i}{dx}f_j dx\right] \qquad \text{(A.17)}$$

$$[S_{qq}]=\left[\int_e \left(f_i f_j+\omega\frac{\Delta x}{2}w_{qq}\frac{df_i}{dx}f_j\right)dx\right]$$

And the stiffness matrix $\mathbf{K}=\sum_{e=1}^{N_e}\mathbf{K}_e$ and $\mathbf{K}_e=\begin{bmatrix}K_{aa} & K_{aq}\\ K_{qa} & K_{qq}\end{bmatrix}$, in which

$$[K_{aa}]=\left[\int_e \omega\frac{\Delta x}{2}w_{aq}\frac{df_i}{dx}\left(a_{qa}\frac{df_j}{dx}\right)dx\right]$$

$$[K_{aq}]=\left[\int_e \left(-f_j\frac{df_i}{dx}+\omega\frac{\Delta x}{2}w_{aa}\frac{df_i}{dx}\frac{df_j}{dx}+\omega\frac{\Delta x}{2}w_{aq}\frac{df_i}{dx}\left(a_{qq}\frac{df_j}{dx}+ff_j\right)\right)dx\right]$$

$$[K_{qa}]=\left[\int_e \left(\omega\frac{\Delta x}{2}w_{qq}\frac{df_i}{dx}\left(a_{qa}\frac{df_j}{dx}\right)\right)dx\right] \qquad \text{(A.18)}$$

$$[K_{qq}]=\left[\int_e \left(-f_j U\frac{df_i}{dx}+ff_i f_j+\omega\frac{\Delta x}{2}w_{qa}\frac{df_i}{dx}\frac{df_j}{dx}+\omega\frac{\Delta x}{2}w_{qq}\frac{df_i}{dx}\left(a_{qq}\frac{df_j}{dx}+ff_j\right)\right)dx\right]$$

The source term $\mathbf{f}=\sum_{e=1}^{N_e}\mathbf{f}_e$ and $\mathbf{f}_e=\begin{Bmatrix}\mathrm{f}_a\\ \mathrm{f}_q\end{Bmatrix}$, in which

$$[\mathrm{f}_a]=\left[f_i f_j Q_j\right]_e-\int_e \omega\frac{\Delta x}{2}w_{aq}\frac{df_i}{dx}\left(\frac{\partial}{\partial x}\left(gI_1-gI_{1\bar{H}}\right)\right)dx$$

$$\left[\mathrm{f}_q\right]=\left[f_i f_j Q_j U\right]_e+\left[f_i\left(gI_1-gI_{1\bar{H}}\right)\right]_e-\int_e \omega\frac{\Delta x}{2}w_{qq}\frac{df_i}{dx}\left(\frac{\partial}{\partial x}\left(gI_1-gI_{1\bar{H}}\right)\right)dx \quad \text{(A.19)}$$

$$+\int_e \left(gI_1-gI_{1\bar{H}}\right)\frac{df_i}{dx}dx$$

As a result of discontinuity of $\bar{H}$ from element to element, the boundary term of element $\left[-gI_{1\bar{H}}\right]_e$ is incapable of offsetting for internal element and will appear in the source term after assembling. The other boundary terms of element disappear during assemble step and only the boundary terms of domain remain. That is

$$\mathbf{f}=\sum_{e=1}^{N_e}\mathbf{f}_e=\left\{\begin{array}{l}\left[f_i f_j Q_j\right]_0^L-\sum_e^{N_e}\int_e \omega\frac{\Delta x}{2}w_{aq}\frac{df_i}{dx}\left(\frac{\partial}{\partial x}\left(gI_1-gI_{1\bar{H}}\right)\right)dx \\ \left[f_i f_j Q_j U+f_i gI_1\right]_0^L+\sum_e^{N_e}\left[-f_i gI_{1\bar{H}}\right]_e-\sum_e^{N_e}\int_e \omega\frac{\Delta x}{2}w_{qq}\frac{df_i}{dx}\left(\frac{\partial}{\partial x}\left(gI_1-gI_{1\bar{H}}\right)\right)dx \\ +\sum_e^{N_e}\int_e \left(gI_1-gI_{1\bar{H}}\right)\frac{df_i}{dx}dx\end{array}\right\}$$

(A.20)

The semi-discrete form (A.16) is then discretized in time by using the θ implicit finite difference approximation.

$$\left(\mathbf{S}+\theta\Delta t\mathbf{K}^{n+1}\right)\Phi^{n+1}=\left(\mathbf{S}-\left(1-\theta\right)\Delta t\mathbf{K}^{n}\right)\Phi^{n}-\theta\Delta t\mathbf{f}^{n+1}+\left(1-\theta\right)\Delta t\mathbf{f}^{n} \qquad \text{(A.21)}$$

The Newton-Raphson iterative method is used to solve them at each time step.

APPENDIX B

DETAILS OF KNOWN FLOW DATA FOR THE 1995 FLOOD EVENT

B.1 Discharge hydrographs on the Oldman River (Units: m3/s)

Date	Oldman dam	Lethbridge	Medicine Hat	Date	Oldman dam	Lethbridge	Medicine Hat
1995/6/1 0:00	282.61	444.05	480.94	1995/6/7 17:00	1434		
1995/6/1 6:00	249.64	487.69	503.24	1995/6/7 18:00	1435	2010.30	846.92
1995/6/1 12:00	222.44	542.66	529.20	1995/6/7 19:00	1438		
1995/6/1 18:00	219.14	562.23	589.81	1995/6/7 20:00	1442		
1995/6/2 0:00	214.90	566.87	685.12	1995/6/7 21:00	1500		
1995/6/2 6:00	211.90	567.37	729.74	1995/6/7 22:00	1500		
1995/6/2 12:00	196.66	577.21	742.83	1995/6/7 23:00	1400		
1995/6/2 18:00	187.69	572.31	784.54	1995/6/8 0:00	1200	3666.15	959.23
1995/6/3 0:00	184.60	559.82	828.61	1995/6/8 1:00	1172		
1995/6/3 6:00	181.80	563.52	853.04	1995/6/8 2:00	1172		
1995/6/3 12:00	179.11	558.62	863.07	1995/6/8 3:00	1067		
1995/6/3 18:00	176.80	557.99	865.73	1995/6/8 4:00	969		
1995/6/4 0:00	173.21	560.50	864.82	1995/6/8 5:00	869		
1995/6/4 6:00	170.52	567.40	873.62	1995/6/8 6:00	775	4386.26	1072.04
1995/6/4 12:00	167.79	573.44	874.35	1995/6/8 12:00	600	4213.48	1430.11
1995/6/4 18:00	165.35	584.14	869.03	1995/6/8 18:00	523	3906.60	1767.46
1995/6/5 0:00	161.56	580.78	867.66	1995/6/9 0:00		3687.89	2695.65
1995/6/5 6:00	140.14	571.88	861.88	1995/6/9 6:00		2962.60	4361.17
1995/6/5 12:00	128.61	572.38	860.51	1995/6/9 12:00		2330.29	5134.50
1995/6/5 18:00	125.30	574.62	866.56	1995/6/9 18:00		1888.04	5345.37
1995/6/6 0:00	122.64	568.99	874.72	1995/6/10 0:00		1787.59	
1995/6/6 6:00	133.72	587.29	886.17	1995/6/10 6:00		1592.08	4401.20
1995/6/6 12:00	166.88		884.52	1995/6/10 12:00	380	1459.76	3810.00
1995/6/6 18:00	319	633.16	880.31	1995/6/10 18:00	380	1321.75	3227.85
1995/6/6 19:00	324			1995/6/11 0:00	380	1236.03	2832.00
1995/6/6 20:00	331			1995/6/11 6:00	380	1139.06	2589.06
1995/6/6 21:00	600			1995/6/11 12:00	350	1080.45	2387.73
1995/6/6 22:00	805			1995/6/11 18:00	326	992.86	2203.73
1995/6/6 23:00	1000			1995/6/12 0:00	324	936.86	2075.37
1995/6/7 0:00	2410	700.20	888.01	1995/6/12 6:00	322	868.14	1987.00
1995/6/7 1:00	2722			1995/6/12 12:00		830.01	1860.84
1995/6/7 2:00	2722			1995/6/12 18:00		794.41	1714.01
1995/6/7 3:00	2517			1995/6/13 0:00		749.27	1585.10
1995/6/7 4:00	2526			1995/6/13 6:00	250.52	732.50	1537.27
1995/6/7 5:00	2554			1995/6/13 12:00		730.76	1459.84
1995/6/7 6:00	2554	1014.88	905.53	1995/6/13 18:00		714.94	1374.51
1995/6/7 7:00	2581			1995/6/14 0:00		709.22	1305.90
1995/6/7 8:00	2586			1995/6/14 6:00	244.91	709.31	1267.88
1995/6/7 9:00	2302			1995/6/14 12:00	242.60	710.63	1235.94
1995/6/7 10:00	1700			1995/6/14 18:00		688.32	1175.95
1995/6/7 11:00	1414			1995/6/15 0:00		672.56	1096.63
1995/6/7 12:00	1421	1444.33	928.05	1995/6/15 6:00	232.70	665.13	1065.22
1995/6/7 13:00	1426			1995/6/15 12:00	215.30	659.80	1069.34
1995/6/7 14:00	1430			1995/6/15 18:00		654.42	1063.97
1995/6/7 15:00	1432			1995/6/16 0:00		648.26	1026.50
1995/6/7 16:00	1433			1995/6/16 6:00	206.30	626.70	971.54

(continued)

Date	Oldman dam	Lethbridge	Medicine	Date	Oldman dam	Lethbridge	Medicine
1995/6/16 12:00	201.20	615.23	950.19	1995/6/23 18:00		469.11	779.18
1995/6/16 18:00		603.06	948.45	1995/6/24 0:00		462.95	763.78
1995/6/17 0:00		586.23	912.73	1995/6/24 6:00		458.06	757.98
1995/6/17 6:00		576.54	886.54	1995/6/24 12:00		456.85	767.71
1995/6/17 12:00		570.67	877.85	1995/6/24 18:00		451.75	771.65
1995/6/17 18:00		562.36	870.99	1995/6/25 0:00		449.72	766.95
1995/6/18 0:00		554.34	843.52	1995/6/25 6:00	160.56	447.23	753.06
1995/6/18 6:00		551.04	795.18	1995/6/25 12:00		445.22	735.43
1995/6/18 12:00		549.97	765.25	1995/6/25 18:00		445.45	728.70
1995/6/18 18:00		546.13	769.68	1995/6/26 0:00	148.16	448.22	730.19
1995/6/19 0:00		540.17	773.39	1995/6/26 6:00	158.07	443.39	741.61
1995/6/19 6:00	195.80	537.81	763.43	1995/6/26 12:00		441.19	749.51
1995/6/19 12:00	166.32	537.54	745.81	1995/6/26 18:00		443.42	733.36
1995/6/19 18:00		530.17	732.52	1995/6/27 0:00		441.39	707.78
1995/6/20 0:00		507.34	720.90	1995/6/27 6:00	170.16	414.61	679.69
1995/6/20 6:00	177.52	466.05	718.45	1995/6/27 12:00	168.00	429.17	662.71
1995/6/20 12:00	170.16	462.31	731.73	1995/6/27 18:00		434.27	674.79
1995/6/20 18:00		457.47	745.32	1995/6/28 0:00		444.33	680.78
1995/6/21 0:00		449.71	736.15	1995/6/28 6:00	154.80	482.20	674.36
1995/6/21 6:00	172.08	461.01	717.13	1995/6/28 12:00	154.32	487.67	657.69
1995/6/21 12:00	172.08	466.15	723.74	1995/6/28 18:00		486.73	665.69
1995/6/21 18:00		465.04	743.00	1995/6/29 0:00		476.87	676.38
1995/6/22 0:00		459.15	745.03	1995/6/29 6:00	150.96	468.47	692.71
1995/6/22 6:00	172.08	452.92	737.75	1995/6/29 12:00	150.96	459.13	710.62
1995/6/22 12:00	172.08	446.65	740.84	1995/6/29 18:00		438.00	716.65
1995/6/22 18:00		447.27	768.57	1995/6/30 0:00		423.43	716.95
1995/6/23 0:00		462.58	785.02	1995/6/30 6:00		414.60	714.19
1995/6/23 6:00	172.08	471.29	791.72	1995/6/30 12:00	151.44	411.30	708.83
1995/6/23 12:00	170.64	464.08	791.16	1995/6/30 18:00		404.00	711.28

B.2 Discharge hydrographs on the tributaries (Units: m3/s)

Date	Belly River	Waterton River	St Mary River	Bow River	Date	Belly River	Waterton River	St Mary River	Bow River
01/06/1995 0:00	61.09	115.87	63.27	289.04	12/06/1995 6:00	59.76	217.83	189.20	429.27
01/06/1995 6:00	64.67	120.45	63.55	337.91	12/06/1995 12:00	62.31	214.32	180.22	405.27
01/06/1995 12:00	61.03	162.46	64.37	346.85	12/06/1995 18:00	65.41	210.81	148.70	417.10
01/06/1995 18:00	56.72	163.47	68.51	377.89	13/06/1995 0:00	65.60	207.30	165.38	421.20
02/06/1995 0:00	55.45	163.39	68.78	382.04	13/06/1995 6:00	66.38	203.79	189.34	375.60
02/06/1995 6:00	55.71	163.76	69.48	381.17	13/06/1995 12:00	72.00	200.28	157.28	294.73
02/06/1995 12:00	54.60	164.49	69.59	399.00	13/06/1995 18:00	60.38	196.78	141.67	304.01
02/06/1995 18:00	52.61	164.97	60.02	425.33	14/06/1995 0:00	60.19	193.27	140.64	324.70
03/06/1995 0:00	51.89	165.35	57.97	422.62	14/06/1995 6:00	59.56	189.76	140.44	306.85
03/06/1995 6:00	52.09	165.52	58.05	430.04	14/06/1995 12:00	60.44	186.25	136.02	294.97
03/06/1995 12:00	51.38	165.85	58.30	441.89	14/06/1995 18:00	59.18	182.74	126.03	224.90
03/06/1995 18:00	49.67	165.90	57.84	488.91	15/06/1995 0:00	58.15	179.23	125.67	273.08
04/06/1995 0:00	48.22	165.91	57.80	434.77	15/06/1995 6:00	56.76	175.73	126.07	234.72
04/06/1995 6:00	47.19	165.98	57.95	439.21	15/06/1995 12:00	53.65	172.22	126.37	223.35
04/06/1995 12:00	45.74	152.08	58.31	460.86	15/06/1995 18:00	53.18	168.71	126.55	224.00
04/06/1995 18:00	44.33	150.62	55.03	488.91	16/06/1995 0:00	52.59	165.20	126.53	250.79
05/06/1995 0:00	44.11	150.77	48.05	498.19	16/06/1995 6:00	52.57	161.69	125.51	247.37
05/06/1995 6:00	40.67	151.04	48.02	498.14	16/06/1995 12:00	51.38	49.04	121.85	199.13
05/06/1995 12:00	34.61	151.44	47.60	516.49	16/06/1995 18:00	49.94	49.50	110.04	183.51
05/06/1995 18:00	35.11	151.82	46.46	518.31	17/06/1995 0:00	48.17	52.09	109.53	209.00
06/06/1995 0:00	37.15	152.47	46.83	514.26	17/06/1995 6:00	48.32	51.10	109.69	219.00
06/06/1995 6:00	46.15	157.30	47.61	511.21	17/06/1995 12:00	48.03	75.07	109.79	214.00
06/06/1995 12:00	93.92	179.95	54.01	518.21	17/06/1995 18:00	47.58	109.84	109.39	197.20
06/06/1995 18:00	177.02	263.37	63.52	525.24	18/06/1995 0:00	47.55	113.58	109.13	187.00
07/06/1995 0:00	279.87	279.94	256.73	534.28	18/06/1995 6:00	48.08	118.24	108.92	175.08
07/06/1995 6:00	252.89	281.23	532.85	589.55	18/06/1995 12:00	47.94	149.60	108.52	178.12
07/06/1995 12:00	198.76	281.59	574.12	738.78	18/06/1995 18:00	47.44	147.05	108.73	199.23
07/06/1995 18:00	159.37	279.85	606.20	958.37	19/06/1995 0:00	47.00	198.87	108.56	218.30
08/06/1995 0:00	131.03	276.93		1124.84	19/06/1995 6:00	47.32	235.65	108.87	210.60
08/06/1995 6:00	127.05	272.96		1081.82	19/06/1995 12:00	46.62	244.42	107.32	202.70
08/06/1995 12:00	163.43	270.59	448.17	1247.60	19/06/1995 18:00	46.22	256.23	98.26	236.87
08/06/1995 18:00	151.31	268.68	465.37	1418.26	20/06/1995 0:00	46.34	261.02	86.52	286.22
09/06/1995 0:00	137.96	262.09	443.46	1265.98	20/06/1995 6:00	45.98	261.02	85.55	290.30
09/06/1995 6:00	125.70	261.55	414.90	1067.24	20/06/1995 12:00	44.72	260.95	84.05	291.89
09/06/1995 12:00	109.06	261.77	396.67	918.01	20/06/1995 18:00	43.33	260.88	73.45	271.83
09/06/1995 18:00	90.89	219.17	349.74	850.99	21/06/1995 0:00	42.20	260.85	78.64	286.84
10/06/1995 0:00	83.49	196.28	352.03	771.52	21/06/1995 6:00	42.00	130.58	79.32	324.30
10/06/1995 6:00	78.61	127.11	344.70	639.15	21/06/1995 12:00	37.08	105.35	79.42	328.27
10/06/1995 12:00	74.41	173.97	304.71	640.07	21/06/1995 18:00	33.89	105.43	79.57	340.28
10/06/1995 18:00	69.70	174.26	266.39	629.51	22/06/1995 0:00	36.15	105.95	76.10	346.00
11/06/1995 0:00	66.28	235.37	259.64	633.39	22/06/1995 6:00	49.29	106.65	73.30	330.43
11/06/1995 6:00	63.86	231.86	252.48	597.95	22/06/1995 12:00	41.43	107.43	73.47	307.41
11/06/1995 12:00	62.30	228.35	223.90	483.79	22/06/1995 18:00	47.75	110.18	73.73	292.28
11/06/1995 18:00	61.05	224.84	193.55	438.94	23/06/1995 0:00	45.59	111.45	73.91	315.23
12/06/1995 0:00	59.68	221.33	191.45	455.82	23/06/1995 6:00	44.19	111.12	74.26	311.95

(continued)

Date	Belly River	Waterton River	St Mary River	Bow River	Date	Belly River	Waterton River	St Mary River	Bow River
23/06/1995 12:00	42.61	111.01	74.80	306.05	27/06/1995 6:00	43.69	107.85	96.52	239.10
23/06/1995 18:00	40.53	110.65	74.97	288.20	27/06/1995 12:00	45.33	121.43	96.27	235.50
24/06/1995 0:00	39.32	110.71	75.05	280.21	27/06/1995 18:00	43.92	127.70	96.82	214.20
24/06/1995 6:00	39.50	112.42	75.50	281.01	28/06/1995 0:00	41.96	127.27	107.97	208.20
24/06/1995 12:00	38.81	111.29	76.03	287.58	28/06/1995 6:00	38.81	124.60	110.01	212.66
24/06/1995 18:00	37.36	114.63	80.53	317.33	28/06/1995 12:00	38.45	119.81	110.45	218.90
25/06/1995 0:00	37.11	114.15	81.57	320.11	28/06/1995 18:00	36.49	113.92	111.20	219.40
25/06/1995 6:00	37.39	113.52	81.61	286.16	29/06/1995 0:00	34.39	110.70	110.06	230.35
25/06/1995 12:00	36.91	110.68	83.53	234.87	29/06/1995 6:00	33.46	109.43	110.12	252.56
25/06/1995 18:00	35.97	110.55	93.67	210.25	29/06/1995 12:00	32.35	106.78	106.48	220.75
26/06/1995 0:00	35.46	110.10	93.77	239.73	29/06/1995 18:00	30.35	107.95	93.68	193.53
26/06/1995 6:00	35.74	109.25	93.81	238.40	30/06/1995 0:00	28.62	107.15	93.51	191.33
26/06/1995 12:00	35.52	102.88	94.74	230.90	30/06/1995 6:00	27.82	105.88	93.60	191.92
26/06/1995 18:00	36.55	104.00	95.99	232.50	30/06/1995 12:00	27.38	94.56	92.30	194.65
27/06/1995 0:00	39.49	104.85	97.09	232.80	30/06/1995 18:00	26.24	84.36	81.61	196.55